Entanglement asymmetry and quantum Mpemba effect in the XY spin chain

OPEN ACCESS

Journal of Statistical Mechanics: Theory and Experiment
An IOP and SISSA journal

PAPER: Quantum statistical physics, condensed matter, integrable systems

Entanglement asymmetry and quantum Mpemba effect in the XY spin chain

Sara Murciano[1,2,*], **Filiberto Ares**[3], **Israel Klich**[4] **and Pasquale Calabrese**[3,5]

[1] Walter Burke Institute for Theoretical Physics, Caltech, Pasadena, CA 91125, United States of America
[2] Department of Physics and IQIM, Caltech, Pasadena, CA 91125, United States of America
[3] SISSA and INFN Sezione di Trieste, via Bonomea 265, 34136 Trieste, Italy
[4] Department of Physics, University of Virginia, Charlottesville, VA, United States of America
[5] International Centre for Theoretical Physics (ICTP), Strada Costiera 11, 34151 Trieste, Italy
E-mail: smurcian@sissa.it

Received 29 October 2023
Accepted for publication 29 November 2023
Published 19 January 2024

Online at stacks.iop.org/JSTAT/2024/013103
https://doi.org/10.1088/1742-5468/ad17b4

Abstract. Entanglement asymmetry is a quantity recently introduced to measure how much a symmetry is broken in a part of an extended quantum system. It has been employed to analyze the non-equilibrium dynamics of a broken symmetry after a global quantum quench with a Hamiltonian that preserves it. In this work, we carry out a comprehensive analysis of the entanglement asymmetry at equilibrium taking the ground state of the XY spin chain, which breaks the $U(1)$ particle number symmetry, and provide a physical interpretation of it in terms of superconducting Cooper pairs. We also consider quenches from this ground state to the XX spin chain, which preserves the $U(1)$ symmetry. In this case, the entanglement asymmetry reveals that the more the symmetry is initially broken, the faster it may be restored in a subsystem, a surprising

*Author to whom any correspondence should be addressed.

and counter-intuitive phenomenon that is a type of a quantum Mpemba effect. We obtain a quasi-particle picture for the entanglement asymmetry in terms of Cooper pairs, from which we derive the microscopic conditions to observe the quantum Mpemba effect in this system, giving further support to the criteria recently proposed for arbitrary integrable quantum systems. In addition, we find that the power law governing symmetry restoration depends discontinuously on whether the initial state is critical or not, leading to new forms of strong and weak Mpemba effects.

Keywords: entanglement entropies, entanglement in extended quantum systems, quantum quenches, spin chains, ladders and planes

J. Stat. Mech. (2024) 013103

Contents

1. Introduction

Hot water may freeze faster than cold water: this counter-intuitive statement describes the Mpemba effect. Such phenomenon was already known to Aristotle and was neglected until 1963 when a student called E B Mpemba observed it preparing an ice-cream [1].

This observation has opened a new research activity devoted to understanding the mechanism and conditions behind the Mpemba effect. Indeed, it has been observed not only in a solution of milk and sugar or in water but in a wide variety of systems, including clathrate hydrates [2], polymers [3], magnetic alloys [4], carbon nanotube resonators [5], granular gases [6], or dilute atomic gases [7] to cite some of them. Today, the Mpemba effect is more generally rephrased as an anomalous relaxation phenomenon where a system initially further out of equilibrium relaxes faster than a system initially closer to equilibrium. Recently, a theoretical framework for the Mpemba effect was developed in [8, 9], followed by a demonstration of the effect in a controlled experimental setting consisting of a colloidal system that is suddenly quenched by placing it in a thermal bath at a lower temperature [10]. Further aspects of this framework have been studied, e.g. in [11–14]. We emphasize that one important aspect of these works is the introduction of a distance between the state of the system and the final equilibrium state to characterize the Mpemba effect.

Despite considerable effort to understand this phenomenon at a classical level, there are only a few investigations in the quantum realm. Most of them study the relaxation of quantum systems after a quench of the temperature or are subject to non-unitary dynamics [15–20]. However, a version of the Mpemba effect in a closed many-body quantum system at zero temperature has been recently reported in [21]. In particular, if we prepare a spin-1/2 chain in a state that breaks a $U(1)$ symmetry and we evolve the system unitarily with a Hamiltonian that preserves it, the symmetry may be dynamically restored in a subsystem of the chain and, furthermore, the more the symmetry is initially broken, the faster it may be restored. The situation here is slightly different from the standard classical Mpemba effect: since the system is isolated, the local equilibrium state does depend on the initial state. Then, what defines the quantum Mpemba effect in this context is not the distance from a common asymptotic state but rather the amount of symmetry breaking.

Thus, in order to study the quantum Mpemba effect, we have to use a quantity that does a similar job as the distance considered in [8, 10] to probe the classical counterpart, but at the level of symmetry breaking. To this aim in [21] the entanglement asymmetry was introduced to measure how much a symmetry is broken in a part of an extended quantum system. So far, the entanglement asymmetry has been studied for the $U(1)$ symmetry associated with transverse magnetization (particle number) in global quantum quenches to the XX spin chain from both the tilted ferromagnetic and Néel states, see [21, 22] respectively. While in the first case, the quantum Mpemba effect can be observed, for the tilted Néel state the symmetry is not restored after the quench since the reduced density matrix relaxes to a non-Abelian generalized Gibbs ensemble. In this case, the asymmetry tends at late times to different non-zero values depending on the initial state, and one cannot define a quantum Mpemba effect. The entanglement asymmetry and the quantum Mpemba effect have also been analyzed in quenches from different initial states to interacting integrable Hamiltonians in the recent [23], in particular, the Lieb–Liniger model and the rule 54 quantum cellular automaton, using the space-time duality approach developed in [24]. In addition, a general explanation of the microscopic origin of the quantum Mpemba effect in free and interacting integrable systems has also been proposed in [23]. Furthermore, experimental

J. Stat. Mech. (2024) 013103

confirmations of this effect have been reported in a trapped-ion setup [25]. Entanglement asymmetry has also been employed to analyze the breaking of discrete symmetries in the XY spin-chain [26] and the massive Ising field theory [27], and of compact groups in matrix product states [28].

The goal of the present paper is twofold. On the one hand, we perform a comprehensive analysis of the entanglement asymmetry in the ground state of the XY spin chain, which is the most paradigmatic free integrable system that breaks a $U(1)$ symmetry. On the other hand, taking this ground state, we investigate the time evolution of the entanglement asymmetry after a sudden global quench to the XX spin chain Hamiltonian, which respects the $U(1)$ symmetry. This framework provides the ideal setup to further study the quantum Mpemba effect discovered in [21] in free fermionic systems and give support to the general mechanism presented in [23] for integrable models.

Entanglement asymmetry: Before summarizing our main results, let us first define the entanglement asymmetry. We consider an extended quantum system in a pure state $|\Psi\rangle$, which we divide into two spatial regions A and B. The state of A is given by the reduced density matrix ρ_A obtained as $\rho_A = \mathrm{Tr}_B(|\Psi\rangle\langle\Psi|)$, where Tr_B denotes the partial trace in the subsystem B. Let us denote by Q the charge operator with integer eigenvalues that generates a $U(1)$ symmetry group. We require that Q is the sum of the charge in each region, $Q = Q_A + Q_B$. If $|\Psi\rangle$ has a defined charge, i.e. it is an eigenstate of Q, then it respects the corresponding symmetry and $[\rho_A, Q_A] = 0$. The latter implies that ρ_A is block-diagonal in the eigenbasis of Q_A and each block corresponds to a particular charge sector. This situation has recently been intensively studied in the context of entanglement since entanglement entropy [29–32] and other entanglement measures [33–36] admit a decomposition in the charge sectors of the theory, which provides a much better understanding of numerous features of quantum many-body systems [37–48].

On the other hand, if $|\Psi\rangle$ is not eigenstate of Q, then it breaks the $U(1)$ symmetry generated by Q and $[\rho_A, Q_A] \neq 0$. Therefore, ρ_A is not block-diagonal. In this case, a proper measure of how much the symmetry is broken in the subsystem A is the entanglement asymmetry, denoted by ΔS_A, and defined as

$$\Delta S_A = S(\rho_{A,Q}) - S(\rho_A), \quad S(\rho) = -\mathrm{Tr}(\rho \log \rho). \tag{1}$$

In this definition, the density matrix $\rho_{A,Q}$ is the result of projecting ρ_A over all the charge sectors of Q_A; that is, $\rho_{A,Q} = \sum_{q\in\mathbb{Z}} \Pi_q \rho_A \Pi_q$, where Π_q denotes the projector onto the eigenspace of Q_A with charge $q \in \mathbb{Z}$. The matrix $\rho_{A,Q}$ is therefore block-diagonal in the eigenbasis of Q_A. One can check that, due to the form of $\rho_{A,Q}$, the entanglement asymmetry ΔS_A is equal to the relative entropy between ρ_A and $\rho_{A,Q}$, $\Delta S_A = \mathrm{Tr}[\rho_A(\log \rho_A - \log \rho_{A,Q})]$ [49]. This identity implies that the entanglement asymmetry is non-negative, $\Delta S_A \geqslant 0$. The other important property as measure of symmetry breaking is that ΔS_A vanishes if and only if $[\rho_A, Q_A] = 0$; that is, when the state of A respects the symmetry associated to Q_A.

J. Stat. Mech. (2024) 013103

The entanglement asymmetry ΔS_A can be computed from the moments of the density matrices ρ_A and $\rho_{A,Q}$ by applying the well-known replica trick for the entanglement entropy [50, 51]. If we define the Rényi entanglement asymmetry as

$$\Delta S_A^{(n)} = S^{(n)}(\rho_{A,Q}) - S^{(n)}(\rho_A), \quad S^{(n)}(\rho) = \frac{1}{1-n}\log \mathrm{Tr}(\rho^n). \tag{2}$$

One has that $\lim_{n\to 1}\Delta S_A^{(n)} = \Delta S_A$. As we will see, $\Delta S_A^{(n)}$ is easier to calculate for positive integer n values, for which it can be measured in ion trap experiments using protocols based on randomized shadows [25, 52–55]. Moreover, $\Delta S_A^{(n)}$ satisfies the two crucial properties to be a measure of symmetry breaking: it is non-negative [56] and is zero if and only if $[\rho_A, Q_A] = 0$.

Main results: As we have already mentioned, the goal of this work is to expand the analysis done in [21] for the tilted ferromagnetic state. We study the entanglement asymmetry in the ground state of the XY spin chain, described by the Hamiltonian

$$H = -\frac{1}{4}\sum_{j=-\infty}^{\infty}\left[(1+\gamma)\sigma_j^x\sigma_{j+1}^x + (1-\gamma)\sigma_j^y\sigma_{j+1}^y + 2h\sigma_j^z\right], \tag{3}$$

where the σ_j^β are the Pauli matrices at the site j, γ is the anisotropy parameter between the couplings in the x and y directions of the spin and h is the value of the external transverse magnetic field. When the anisotropy parameter γ is not zero, H breaks the $U(1)$ symmetry generated by the transverse magnetization

$$Q = \frac{1}{2}\sum_j \sigma_j^z. \tag{4}$$

Therefore, in this work, we are interested in the region $\gamma \neq 0$ for which the ground state entanglement asymmetry associated to Q is non-zero while for $\gamma = 0$ it vanishes. For $\gamma \neq 0$, the XY spin chain is critical along the lines $|h| = 1$, which belong to the Ising universality class. The tilted ferromagnetic states considered in [21] are only a subset of the ground states of the Hamiltonian (3) along the curve $\gamma^2 + h^2 = 1$ [57, 58]. In this more general setup, we can compute the entanglement asymmetry for any ground state of (3) and we find that, for a subsystem A of contiguous spins of length ℓ, it reads

$$\Delta S_A^{(n)} = \frac{1}{2}\log\ell + \frac{1}{2}\log\frac{\pi\, g(\gamma,h)\, n^{1/(n-1)}}{4} + O(\ell^{-1}), \tag{5}$$

where $g(\gamma, h)$ is a function depending on the two parameters γ and h of the Hamiltonian (3). We find that this term is related to the density of Cooper pairs, which are responsible for the breaking of the conservation of the number of particles. We remark that $\Delta S_A^{(n)}$ increases logarithmically with the subsystem size, both if the system is critical ($|h| = 1$) or not.

If we choose the ground state of the Hamiltonian in equation (3) for arbitrary γ and h and we let it evolve with the XX spin chain, that is taking $\gamma = 0$ and $h = 0$

J. Stat. Mech. (2024) 013103

in equation (3), which commutes with the charge (4), the symmetry is dynamically restored. We derive a quasi-particle picture for the entanglement asymmetry at large times after the quench based on the initial density of Cooper pairs. From it, we find that the Rényi entanglement asymmetry vanishes for large times as t^{-3} for any initial value of γ when $|h| \neq 1$ and we predict under which conditions for the parameters (γ, h) we observe the Mpemba effect. It turns out that, if the density of Cooper pairs around the slowest modes of the post-quench Hamiltonian is larger for the state that initially breaks less the symmetry, the quantum Mpemba effect occurs, in agreement with the general findings of [23] for integrable systems. On the other hand, when the system is prepared initially in the critical ground state, i.e. $|h| = 1$, the Rényi asymmetry vanishes as t^{-1} for any value of γ. Therefore, for critical systems, we can define a *strong* version of the Mpemba effect for which the relaxation happens algebraically slower regardless of the initial condition for the non-critical state.

Outline: In section 2, we provide a recipe to evaluate the entanglement asymmetry for Gaussian fermionic operators such as the reduced density matrix of the ground state of the XY spin chain. Section 3 is devoted to the analysis of the entanglement asymmetry in the ground state of the XY model, while section 4 studies the time-evolution of the asymmetry after a quench to the XX spin chain and the origin of the Mpemba effect. Finally, we draw our conclusions in section 5 and we include three appendices with additional results and technical details.

2. Charged moments and XY spin chain

As we have seen in the previous section, by applying the replica trick, the entanglement asymmetry ΔS_A can be computed from the Rényi version $\Delta S_A^{(n)}$ defined in equation (2). The advantage of doing this is that, using the Fourier representation of the projector Π_q, the projected density matrix $\rho_{A,Q}$ can be rewritten as

$$\rho_{A,Q} = \int_{-\pi}^{\pi} \frac{\mathrm{d}\alpha}{2\pi} \mathrm{e}^{-i\alpha Q_A} \rho_A \mathrm{e}^{i\alpha Q_A}. \tag{6}$$

Therefore, its moments are given by

$$\mathrm{Tr}\left(\rho_{A,Q}^n\right) = \int_{-\pi}^{\pi} \frac{\mathrm{d}\alpha_1 \ldots \mathrm{d}\alpha_n}{(2\pi)^n} Z_n(\boldsymbol{\alpha}), \tag{7}$$

where $\boldsymbol{\alpha} = \{\alpha_1, \ldots, \alpha_n\}$ and $Z_n(\boldsymbol{\alpha})$ are the (generalized) charged moments

$$Z_n(\boldsymbol{\alpha}) = \mathrm{Tr}\left[\prod_{j=1}^{n} \rho_A \mathrm{e}^{i\alpha_{j,j+1}Q_A}\right], \tag{8}$$

with $\alpha_{ij} \equiv \alpha_i - \alpha_j$ and $\alpha_{n+1} = \alpha_1$. Since in general $[\rho_A, Q_A] \neq 0$, the order in which these operators enter in the expression of $Z_n(\boldsymbol{\alpha})$ is crucial. In fact, if $[\rho_A, Q_A] = 0$, then $Z_n(\boldsymbol{\alpha}) = Z_n(\mathbf{0})$, which implies $\mathrm{Tr}(\rho_{A,Q}^n) = \mathrm{Tr}(\rho_A^n)$ and $\Delta S_A^{(n)} = 0$.

J. Stat. Mech. (2024) 013103

In this manuscript, we are particularly interested in calculating the charged moments $Z_n(\boldsymbol{\alpha})$ and, from them using equation (7), the Rényi entanglement asymmetry $\Delta S_A^{(n)}$ in the ground state of the XY spin chain (3). As well-known, this Hamiltonian is easily diagonalizable as follows [59]. We can first map it to the fermionic operators $\boldsymbol{c}_j = (c_j^\dagger, c_j)$ via a Jordan–Wigner transformation, namely

$$H = -\frac{1}{2}\sum_{j=-\infty}^{\infty}\left(c_j^\dagger c_{j+1} + \gamma c_j^\dagger c_{j+1}^\dagger + \text{h.c} + 2h c_j^\dagger c_j\right). \tag{9}$$

By performing now a Fourier transformation to momentum space $d_k = \sum_{j\in\mathbb{Z}} \mathrm{e}^{-ikj} c_j$ and then the Bogoliubov transformation

$$\begin{pmatrix} \eta_k \\ \eta_{\pi-k} \end{pmatrix} = \begin{pmatrix} \cos(\Delta_k/2) & i\sin(\Delta_k/2) \\ i\sin(\Delta_k/2) & \cos(\Delta_k/2) \end{pmatrix} \begin{pmatrix} d_k \\ d_{\pi-k} \end{pmatrix}, \tag{10}$$

with

$$\begin{aligned} \cos\Delta_k &= \frac{h-\cos(k)}{\sqrt{(h-\cos(k))^2+\gamma^2\sin^2 k}}, \\ \sin\Delta_k &= \frac{\gamma\sin(k)}{\sqrt{(h-\cos(k))^2+\gamma^2\sin^2 k}}, \end{aligned} \tag{11}$$

the XY spin chain is diagonal in terms of the Bogoliubov modes η_k,

$$H = \sum_k \epsilon_k\left(\eta_k^\dagger\eta_k - \frac{1}{2}\right), \tag{12}$$

where ε_k is the single-particle dispersion relation

$$\epsilon_k = \sqrt{(h-\cos k)^2+\gamma^2\sin^2 k}. \tag{13}$$

Thus the ground state is the Bogoliubov vacuum $|0\rangle$ that is annihilated by all the operators η_k, i.e. $\eta_k|0\rangle = 0$ for all k. For $\gamma \neq 0$, this state breaks the $U(1)$ symmetry associated to the conservation of the total transverse magnetization (4), i.e. $[\rho, Q] \neq 0$ with $\rho = |0\rangle\langle 0|$, and the asymmetry $\Delta S_A^{(n)}$ is non-zero. On the other hand, for $\gamma = 0$, $|0\rangle$ is an eigenstate of Q and $\Delta S_A^{(n)}$ vanishes. Therefore, $|0\rangle$ is an ideal state to explore $\Delta S_A^{(n)}$.

The ground state of the XY spin chain is a Slater determinant and, consequently, the reduced density matrix ρ_A is a Gaussian operator in terms of $\boldsymbol{c}_j$ [60]. This simplifies the calculation of $\Delta S_A^{(n)}$ since, due to the Wick's theorem, ρ_A is univocally determined by the two-point correlation matrix

$$\Gamma_{jj'} = 2\mathrm{Tr}\left[\rho_A \boldsymbol{c}_j^\dagger \boldsymbol{c}_{j'}\right] - \delta_{jj'}, \tag{14}$$

J. Stat. Mech. (2024) 013103

with $j, j' \in A$. If A is an interval of contiguous sites of length ℓ, then Γ is a $2\ell \times 2\ell$ block Toeplitz matrix; that is, their entries are the Fourier coefficients [61]

$$\Gamma_{jj'} = \int_0^{2\pi} \frac{\mathrm{d}k}{2\pi} \mathcal{G}(k)\, \mathrm{e}^{-ik(j-j')}, \quad j, j' = 1, \ldots, \ell, \tag{15}$$

of the 2×2 symbol

$$\mathcal{G}(k) = \begin{pmatrix} \cos\Delta_k & -i\sin\Delta_k \\ i\sin\Delta_k & -\cos\Delta_k \end{pmatrix}. \tag{16}$$

Under the Jordan–Wigner transformation, the transverse magnetization Q in equation (4) is mapped to the fermion number operator $Q = \sum_j (c_j^\dagger c_j - 1/2)$ and $\mathrm{e}^{i\alpha Q_A}$ turns out to be Gaussian, too. Therefore, equation (8) is the trace of the product of Gaussian fermionic operators, ρ_A and $\mathrm{e}^{i\alpha_{j,j+1} Q_A}$. As explicitly shown in appendix B of [22], using the special properties of Gaussian operators [62, 63], the trace of equation (8) can be re-expressed as a determinant involving the two-point correlation matrix Γ,

$$Z_n(\boldsymbol{\alpha}) = \sqrt{\det\left[\left(\frac{I-\Gamma}{2}\right)^n \left(I + \prod_{j=1}^{n} W_j\right)\right]}, \tag{17}$$

with $W_j = (I+\Gamma)(I-\Gamma)^{-1}\mathrm{e}^{i\alpha_{j,j+1} n_A}$ and n_A is a diagonal matrix with $(n_A)_{2j,2j} = 1$, $(n_A)_{2j-1,2j-1} = -1$, $j = 1, \ldots, \ell$. Equation (17) allows to exactly compute numerically $\Delta S_A^{(n)}$ and is the starting point to derive analytic expressions for $Z_n(\boldsymbol{\alpha})$ and $\Delta S_A^{(n)}$ for large subsystem sizes.

3. Entanglement asymmetry in the ground state of the XY spin chain

In this section, we study the entanglement asymmetry in the ground state of the XY spin chain. As we have previously shown, this state is the vacuum $|0\rangle$ of the Bogoliubov modes that diagonalize the Hamiltonian (3) of the chain. Since the reduced density matrix $\rho_A = \mathrm{Tr}_B(|0\rangle\langle 0|)$ is Gaussian, we can apply equation (17) to study both numerically and analytically the charged moments $Z_n(\boldsymbol{\alpha})$, from which the Rényi entanglement asymmetry can be derived using equations (2) and (7).

3.1. Charged moments

For simplicity, let us first consider the case $n = 2$ and afterwards we will generalize the results to any n. Observe that, for $n = 2$, the expression (17) of the charged moments $Z_n(\boldsymbol{\alpha})$ in terms of the two-point correlation function Γ simplifies, after a change of variable $\alpha_{12} = \alpha$, as

$$Z_2(\alpha) = \sqrt{\det\left(\frac{I + \Gamma_\alpha \Gamma_{-\alpha}}{2}\right)}. \tag{18}$$

J. Stat. Mech. (2024) 013103

The matrix $\Gamma_\alpha \equiv \Gamma e^{i\alpha n_A}$ is block Toeplitz

$$(\Gamma_\alpha)_{jj'} = \int_{-\pi}^{\pi} \frac{\mathrm{d}k}{2\pi} \mathcal{G}_\alpha(k)\, \mathrm{e}^{-ik(j-j')}, \quad j, j' = 1, \ldots, \ell, \tag{19}$$

with symbol

$$\mathcal{G}_\alpha(k) = \begin{pmatrix} \mathrm{e}^{i\alpha}\cos\Delta_k & -i\,\mathrm{e}^{-i\alpha}\sin\Delta_k \\ i\mathrm{e}^{i\alpha}\sin\Delta_k & -\mathrm{e}^{-i\alpha}\cos\Delta_k \end{pmatrix}. \tag{20}$$

Therefore, in equation (18), we have the product $\Gamma_\alpha\Gamma_{-\alpha}$ of two block Toeplitz matrices, which in general is not block Toeplitz, and the well-known results on the determinant of this kind of matrices cannot in principle be applied. However, in [22], we found the following result for the asymptotic behavior of determinants that contain a product of block Toeplitz matrices like the one in equation (18). If we denote as $T_\ell[g]$ the $(\ell d) \times (\ell d)$ dimensional block Toeplitz matrix with symbol the $d \times d$ matrix g, then for large ℓ

$$\det\left(I + \prod_{j=1}^{n} T_\ell[g_j]\right) \sim \mathrm{e}^{\ell A}, \tag{21}$$

where the coefficient A is given by

$$A = \int_0^{2\pi} \frac{\mathrm{d}k}{2\pi} \log\det\left[I + \prod_{j=1}^{n} g_j(k)\right]. \tag{22}$$

If we apply equation (21) in equation (18), then we obtain that the $n = 2$ charged moments behave for large subsystem size ℓ as

$$Z_2(\alpha) \sim Z_2(0)\, \mathrm{e}^{A_2(\alpha)\ell}, \tag{23}$$

and

$$A_2(\alpha) = \int_{-\pi}^{\pi} \frac{\mathrm{d}k}{4\pi} \log\left(1 - \sin^2\alpha \sin^2\Delta_k\right). \tag{24}$$

In figure 1, we numerically test this result. We plot the logarithm of the ground state charged moment $Z_2(\alpha)/Z_2(0)$ as a function of the angle α for a fixed subsystem of length $\ell = 40$ and two different sets of values for h and γ; in the left panel, we consider $h = \gamma = 0.5$ while in the right one we take $h = 2$ and $\gamma = 0.5$. The dots are the exact value of $Z_2(\alpha)$ calculated using equation (18) and the solid lines correspond to the asymptotic analytic prediction of equation (23). As evident in the plot, for $|h| \leqslant 1$, $\log(Z_2(\alpha)/Z_2(0))$ presents a cusp at $\alpha = \pm\pi/2$ while, for $|h| > 1$, this non-analiticity disappears. In the inset of the right panel, we check that the discrepancy between the analytic prediction and the exact points around $\alpha = \pi/2$ is due to subleading corrections in ℓ, see the caption for details.

https://doi.org/10.1088/1742-5468/ad17b4

J. Stat. Mech. (2024) 013103

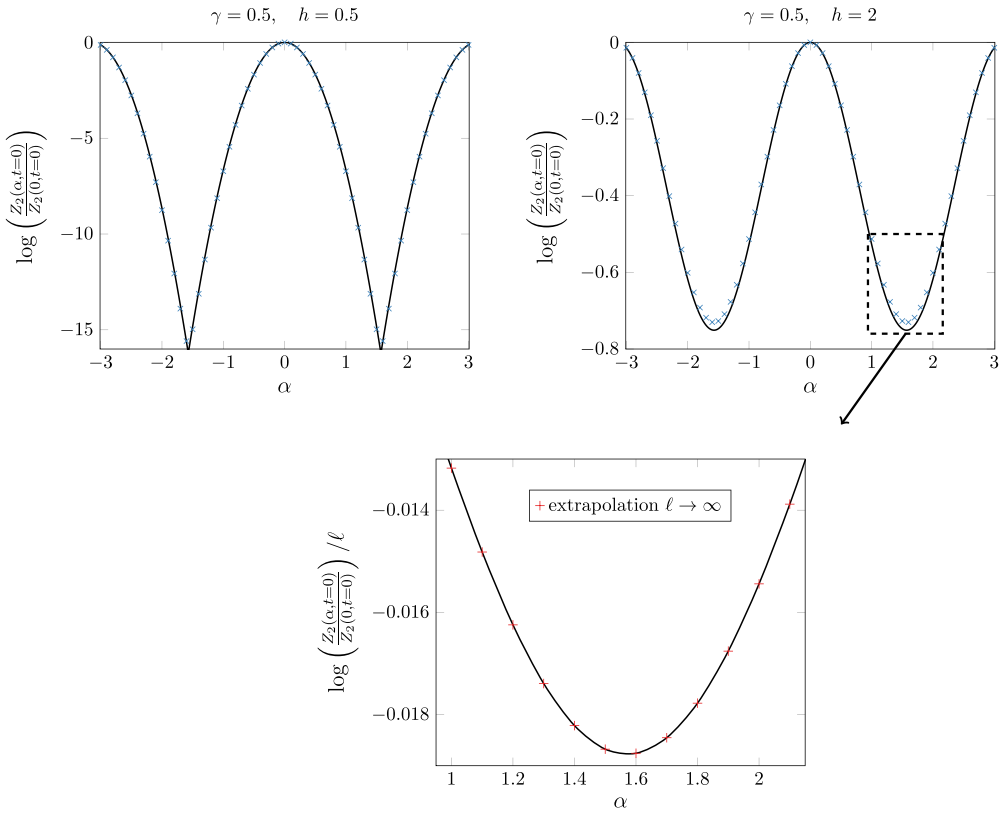

Figure 1. Logarithm of the $n = 2$ charged moment $Z_2(\alpha)/Z_2(0)$ in the ground state of the XY spin chain as a function of α for different values of h and γ and subsystem size $\ell = 40$. The solid lines correspond to the analytic prediction of equation (27) while the points are the exact values obtained using directly equation (18). The bottom panel represents the extrapolated data with extrapolation form $a + b/\ell$ to check that the discrepancy observed in the right panel is only a finite-size effect. To extrapolate the data, we have taken into account the numerical data for $\ell = 40, 50, 60$. Interestingly, the extrapolated points are exactly equal to our analytical prediction of the linear growth of $\log Z_2(\alpha)$ in equation (27) (solid curve).

The result of equation (23) for $n = 2$ can be rewritten in a more appealing form that straightforwardly suggests its generalization to any integer $n \geqslant 2$. In fact, observe that the coefficient $A_2(\alpha)$ of equation (24) can be recast in the following factorized expression

$$A_2(\alpha) = \int_{-\pi}^{\pi} \frac{\mathrm{d}k}{4\pi} \log\left(f(\cos\Delta_k, \alpha)\, f(\cos\Delta_k, -\alpha)\right) \tag{25}$$

where

$$f(\lambda, \alpha) = i\lambda \sin(\alpha) + \cos(\alpha). \tag{26}$$

As we show in appendix A, this result can be extended to any integer $n \geqslant 2$. The charged moments behave for large ℓ similarly to the case $n=2$, cf equation (23),

$$Z_n(\boldsymbol{\alpha}) \sim Z_n(\mathbf{0})\, \mathrm{e}^{\ell A_n(\boldsymbol{\alpha})}, \tag{27}$$

where the coefficient $A_n(\boldsymbol{\alpha})$ admits the following factorization in the replica space,

$$A_n(\boldsymbol{\alpha}) = \int_0^{2\pi} \frac{\mathrm{d}k}{4\pi} \log \prod_{j=1}^{n} f(\cos\Delta_k, \alpha_{j,j+1}). \tag{28}$$

In figure 2, we check numerically equation (27) for the case $n=3$.

We consider the ratio $Z_3(\alpha_1,\alpha_2,\alpha_3)/Z_3(0,0,0)$ as a function of α_2 for given values of α_1 and α_3. Its real and imaginary parts are plotted respectively in the upper and lower panels for two different sets of couplings h and γ: $h=0.2$, $\gamma=0.5$ on the left and $h=1.2$ and $\gamma=0.5$ on the right. We obtain an excellent agreement. As in the case $n=2$, the logarithm of $Z_3(\alpha_1,\alpha_2,\alpha_3)/Z_3(0,0,0)$ presents cusps when $|h| \leqslant 1$ that disappear in the phase $|h|>1$.

It is important to remark that, along the critical lines $|h|=1$, we have numerically observed that the expression (8) for the charged moments $Z_n(\boldsymbol{\alpha})$ includes an additional subleading term $Z_n(\boldsymbol{\alpha}) \sim Z_n(\mathbf{0})\mathrm{e}^{A_n(\boldsymbol{\alpha})\ell}\ell^{m_n(\boldsymbol{\alpha})}$. Unfortunately, the explicit form of $m_n(\boldsymbol{\alpha})$ cannot be obtained with the methods employed in this manuscript. However, since the factor $\ell^{m_n(\boldsymbol{\alpha})}$ produces a subleading term in the entanglement asymmetry, we can safely neglect it in the rest of the paper.

3.2. Asymptotic behavior of the entanglement asymmetry

As we explain in section 2, once we have the charged moments (8), the Rényi entanglement asymmetry $\Delta S_A^{(n)}$ can be determined by plugging them into the the n-dimensional integral of equation (7) and then using equation (2). In general, this integral can only be calculated by numerical means but, employing a saddle point approximation, we can derive analytically the asymptotic behavior of $\Delta S_A^{(n)}$ for large subsystems.

To do so, we can follow the same strategy applied in [22]. By taking into account that the phases α_{jj+1} satisfy $\sum_{j=1}^{n}\alpha_{jj+1}=0$, we can reduce the n-fold integral (7) to an $(n-1)$-fold one after the change of variables $\tilde{\alpha}_j=\alpha_{jj+1}$,

$$\mathrm{Tr}\left(\rho_{A,Q}^n\right) = \int_{-\pi}^{\pi} \frac{\mathrm{d}\tilde{\alpha}_1 \ldots \mathrm{d}\tilde{\alpha}_{n-1}}{(2\pi)^{n-1}} \mathrm{Tr}\left(\rho_A \mathrm{e}^{i\tilde{\alpha}_1 Q_A} \rho_A \mathrm{e}^{i\tilde{\alpha}_2 Q_A} \cdots \rho_A \mathrm{e}^{-i\sum_{j=1}^{n-1}\tilde{\alpha}_j Q_A}\right). \tag{29}$$

If we insert in this expression the prediction of equation (27) for the charged moments at large ℓ, the integral takes the form

$$\frac{\mathrm{Tr}\left(\rho_{A,Q}^n\right)}{\mathrm{Tr}\left(\rho_A^n\right)} \sim \int_{-\pi}^{\pi} \frac{\mathrm{d}\tilde{\alpha}_1 \cdots \mathrm{d}\tilde{\alpha}_{n-1}}{(2\pi)^{n-1}} \mathrm{e}^{\ell\left[\sum_{j=1}^{n-1} A_1(\tilde{\alpha}_j) + A_1\left(-\sum_{j=1}^{n-1}\tilde{\alpha}_j\right)\right]}, \tag{30}$$

J. Stat. Mech. (2024) 013103

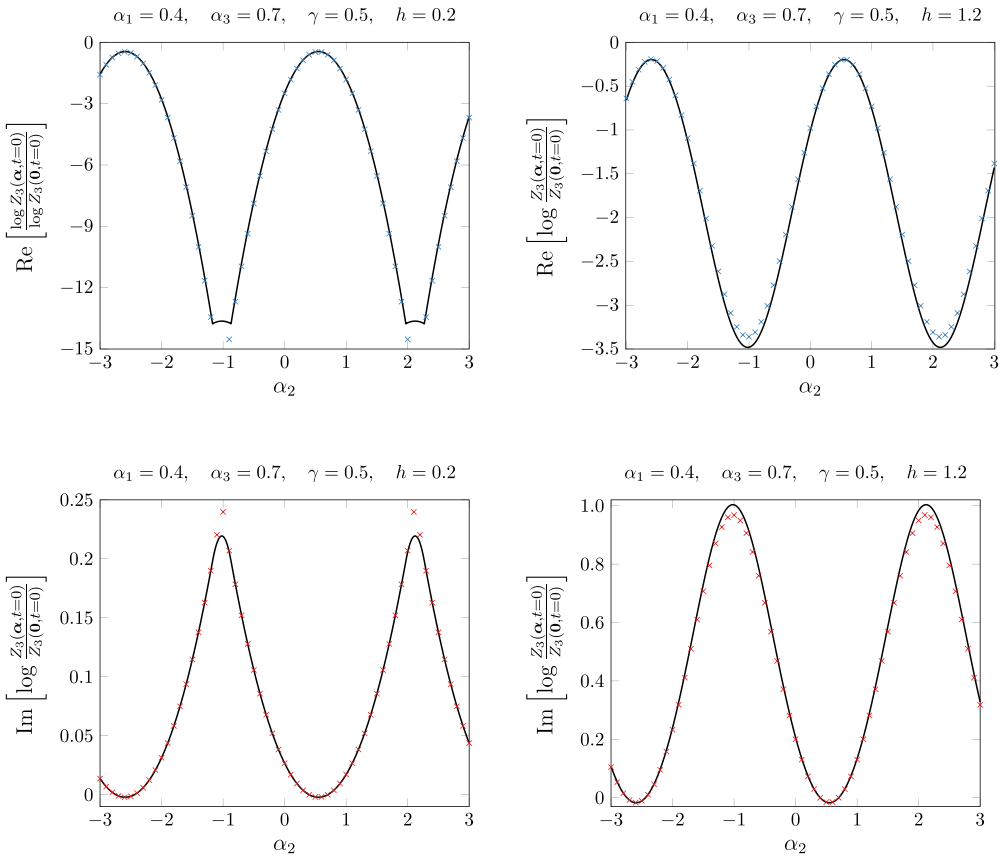

Figure 2. Logarithm of the $n=3$ charged moment $Z_3(\alpha_1,\alpha_2,\alpha_3)/Z_3(0,0,0)$ in the ground state of the XY spin chain as a function of α_2 for α_1 and α_3 constant, different values of the couplings h and γ and subsystem size $\ell = 40$. In the upper panels, we take its real part while the corresponding imaginary part is represented in the plots of the lower row. The points correspond to the exact numerical values calculated using equation (17). The solid lines correspond to the asymptotic expression of equation (27) employing as coefficient $A_3(\boldsymbol{\alpha})$ the prediction of equation (28).

where we have explicitly used the factorization in the replica space found in equation (28) for the coefficient $A_n(\boldsymbol{\alpha})$. One can check that there are 2^{n-1} points in the region of integration $[-\pi,\pi]^{\times(n-1)}$ that satisfy the saddle point condition

$$\partial_{\tilde{\alpha}_i}\left[\sum_{j=1}^{n-1} A_1\left(\tilde{\alpha}_j\right) + A_1\left(-\sum_{j=1}^{n-1}\tilde{\alpha}_j\right)\right] = 0. \tag{31}$$

Around all the saddle points, the integrand of equation (30) has the same behavior at quadratic order in $\tilde{\alpha}_j$ and, therefore, their leading contribution to the integral is the same. Hence, if we expand the exponent in equation (30) around $\tilde{\alpha}_j = 0$ and we

J. Stat. Mech. (2024) 013103

properly count the number of saddle points, then equation (30) can be approximated by the Gaussian integral

$$\frac{\mathrm{Tr}\left(\rho_{A,Q}^{n}\right)}{\mathrm{Tr}\left(\rho_{A}^{n}\right)} \sim 2^{n-1} \int_{-\infty}^{\infty} \frac{\mathrm{d}\tilde{\alpha}_1 \cdots \mathrm{d}\tilde{\alpha}_{n-1}}{(2\pi)^{n-1}} \mathrm{e}^{-\frac{\ell g(\gamma,h)}{2}\left(\sum_{j=1}^{n-1}\tilde{\alpha}_j^2+\sum_{j<j'}\tilde{\alpha}_j\tilde{\alpha}_{j'}\right)}, \tag{32}$$

with

$$g(\gamma,h) = \int_0^{2\pi} \frac{\mathrm{d}k}{2\pi} \sin^2 \Delta_k. \tag{33}$$

The integral of equation (32) is solvable using the standard formulae,

$$\frac{\mathrm{Tr}\left(\rho_{A,Q}^{n}\right)}{\mathrm{Tr}\left(\rho_{A}^{n}\right)} = \frac{2^{n-1}}{\left(\pi\,\ell g(\gamma,h)\right)^{(n-1)/2} n^{1/2}} + O\left(\ell^{-(n+1)/2}\right). \tag{34}$$

Finally, plugging this result in equation (2), we obtain that for the ground state of the XY spin chain, the Rényi entanglement asymmetry behaves as

$$\Delta S_A^{(n)} = \frac{1}{2}\log \ell + \frac{1}{2}\log \frac{\pi\, g(\gamma,h)\, n^{1/(n-1)}}{4} + O\left(\ell^{-1}\right). \tag{35}$$

The integral of equation (33) that gives the term $g(\gamma,h)$ can be computed explicitly. In fact, if we perform the change of variables $z = \mathrm{e}^{ik}$, it can be rewritten as a contour integral in the complex z-plane. Using then the residue theorem, we find

$$g(\gamma,h) = \begin{cases} \frac{\gamma}{\gamma+1}, & |h| \leqslant 1, \\ \frac{\gamma^2}{1-\gamma^2}\left(\frac{|h|}{\sqrt{h^2+\gamma^2-1}} - 1\right), & |h| > 1. \end{cases} \tag{36}$$

In figures 3 and 4, we investigate the validity of equation (35) for $n=2$ and $n=3$ respectively. In these plots, we represent the ground state entanglement asymmetry as a function of the subsystem size taking different couplings h and γ. The points are the exact numerical values of $\Delta S_A^{(n)}$ calculated with equation (17). The dashed lines correspond to assume the prediction of equation (27) for the charged moments and then calculate numerically its exact Fourier transform (7) to get $\Delta S_A^{(n)}$. In this case, we obtain a good agreement with the numerical points for all the values of h and γ considered. The solid lines represent the asymptotic behavior obtained in equation (34) using the saddle point approximation. Observe that, for the range of subsystem sizes considered, equation (35) describes well the exact numerical results for $|h| \leqslant 1$ and any γ, both at $n=2$ and $n=3$. The same occurs for $|h|>1$ and $\gamma>1$. However, for $|h|>1$ and $\gamma<1$, the saddle point approximation requires to consider larger subsystems.

In figure 5, we plot the saddle point approximation of equation (35) for ΔS_A as a function of γ and several fixed values of h (left panel) and viceversa (right panel) taking as susbsystem size $\ell = 1000$ in both cases. Observe in the left panel that ΔS_A grows monotonically with the anisotropy parameter γ. Therefore, by varying γ, we can tune

J. Stat. Mech. (2024) 013103

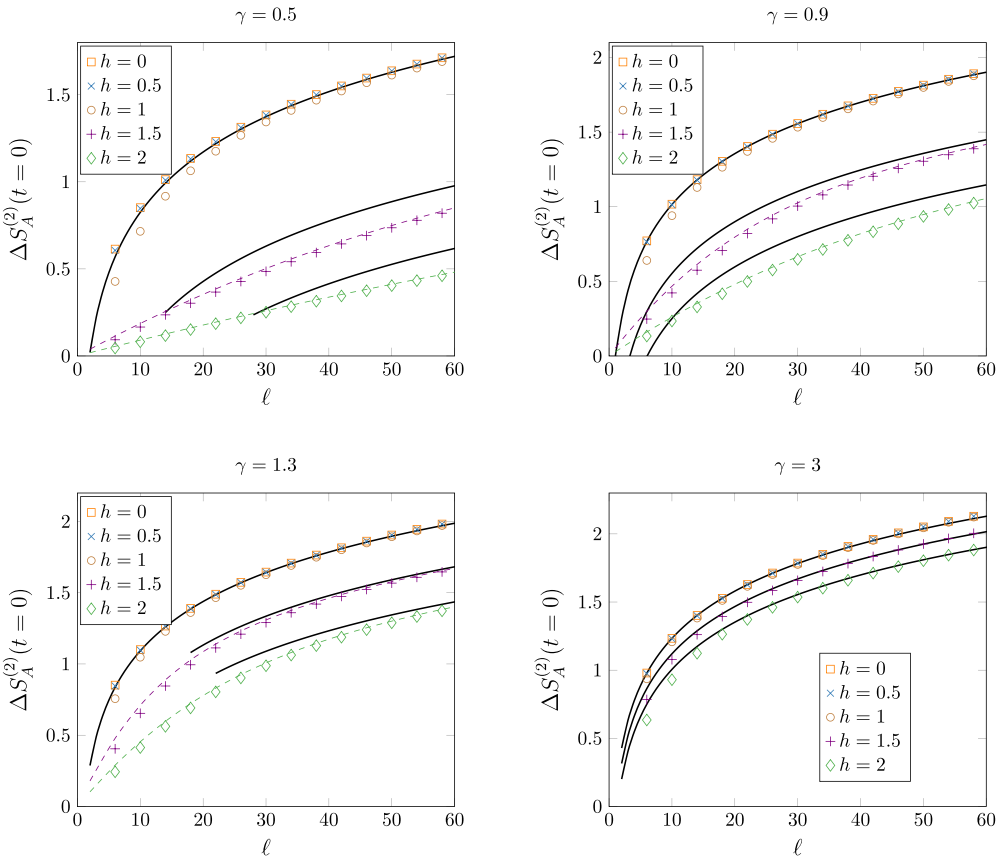

Figure 3. Rényi entanglement asymmetry $\Delta S_A^{(2)}$ as a function of the subsystem length ℓ for different values of h and γ. The dots are the exact numerical values of the asymmetry computed using equation (17). The solid lines correspond to the asymptotic result of equation (35) while the dashed ones correspond to the evaluation of $\Delta S_A^{(2)}$ without the saddle point approximation in the Fourier transformation (7) of the charged moments (27).

how much the $U(1)$ symmetry generated by Q is broken. In particular, as we already pointed out, at $\gamma = 0$, the Hamiltonian (3) corresponds to the XX spin chain which commutes with Q. Hence the ground state respects the corresponding $U(1)$ symmetry and the entanglement asymmetry is expected to vanish. However, according to the asymptotic expression (35), $\Delta S_A \to -\infty$ when $\gamma \to 0$. The reason of this apparent discrepancy is that the limits $\ell \to \infty$ and $\gamma \to 0$ do not commute. The other remarkable property of the ground state entanglement asymmetry can be seen in the right panel. As evident also from equation (36), for large ℓ, the entanglement asymmetry is independent of the transverse magnetic field h in the ferromagnetic phase ($|h| < 1$) while, in the paramagnetic phase ($|h| > 1$), it monotonically decreases with h. In fact, at $h \to \pm\infty$, the ground state of the XY spin chain is $|\uparrow\uparrow\cdots\uparrow\rangle$ and $|\downarrow\downarrow\cdots\downarrow\rangle$ respectively, which are eigenstates of Q, and $\Delta S_A^{(n)} = 0$. When we take this limit in the asymptotic expression (35), the entanglement asymmetry diverges $\Delta S_A^{(n)} \to -\infty$ since the limits $\ell \to \infty$ and $h \to \pm\infty$ do not commute, similarly to the case $\gamma \to 0$.

J. Stat. Mech. (2024) 013103

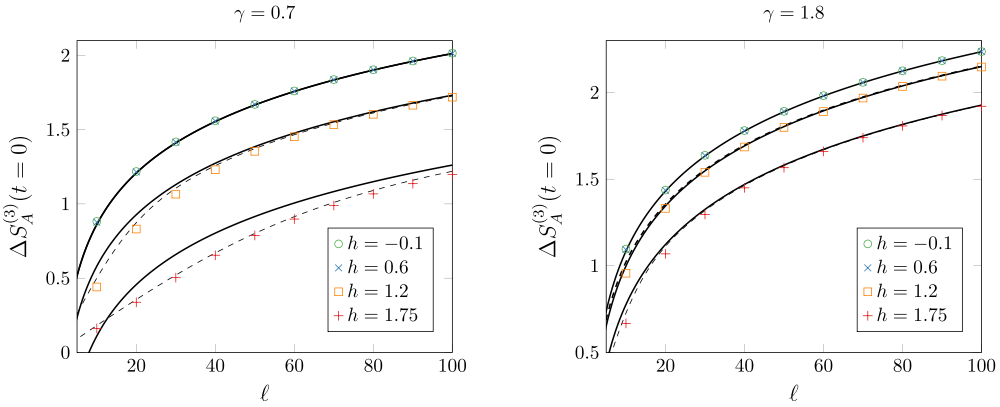

Figure 4. Rényi entanglement asymmetry $\Delta S_A^{(3)}$ for the ground state of the XY spin chain as a function of ℓ for different values of h and γ. The points represent the exact numerical value obtained with equation (17). The solid lines are the result of equation (35) for large subsystem sizes while the dashed ones have been obtained calculating exactly the Fourier transformation (7) of the charged moments $Z_n(\boldsymbol{\alpha})$ using their analytic expression (27).

Finally, it is interesting to note that the asymptotic result (35) for $\Delta S_A^{(n)}$ admits an interpretation in terms of the density of Cooper pairs in the ground state $|0\rangle$. Observe that the factor $g(\gamma,h)$ that enters in equation (35) only depends, as an integral in momentum space, on the quantity $\sin^2\Delta_k$, see equation (33). Using the two-point correlation matrix Γ of equation (15), it is easy to see that $\sin\Delta_k$ is related to the correlator $\langle d^\dagger_{\pi-k} d^\dagger_k\rangle$ by the equality $\langle d^\dagger_{\pi-k} d^\dagger_k\rangle = i\sin\Delta_k/2$. The modulus $|\langle d^\dagger_{\pi-k} d^\dagger_k\rangle|$ can be thought as the density of Cooper pairs of momentum k that the state $|0\rangle$ contains. Therefore, since $\Delta S_A^{(n)}$ is proportional to the logarithm of $\ell g(\gamma,h)$ according to equation (35), it monotonically increases with the density of Cooper pairs present in the state $|0\rangle$ and the $U(1)$ symmetry associated to particle conservation is more broken. In fact, this symmetry is respected if and only if the correlations $\langle d^\dagger_{\pi-k} d^\dagger_k\rangle$ vanish, i.e. in the absence of Cooper pairs. This interpretation of Cooper pairs as the excitations responsible of how much the particle number symmetry is broken will be further supported in the next section, where we elaborate a quasi-particle picture for the entanglement asymmetry after a quench in terms of them.

4. Entanglement asymmetry out-of-equilibrium

In this section, we study the global quantum quench from the ground state of the XY spin chain (3) with $\gamma\neq 0$, $|\Psi(0)\rangle = |0\rangle$, which breaks the particle number symmetry generated by Q, to the XX spin chain Hamiltonian $H_{\rm XX}$, which corresponds to take $\gamma = 0$ and $h = 0$ in equation (3) and, therefore, it commutes with Q and the $U(1)$ symmetry is expected to be dynamically restored in the subsystem A, i.e. $\lim_{t\to\infty}[\rho_A(t), Q_A] = 0$. Thus the time-evolved state is

$$|\Psi(t)\rangle = e^{-itH_{\rm XX}}|\Psi(0)\rangle. \tag{37}$$

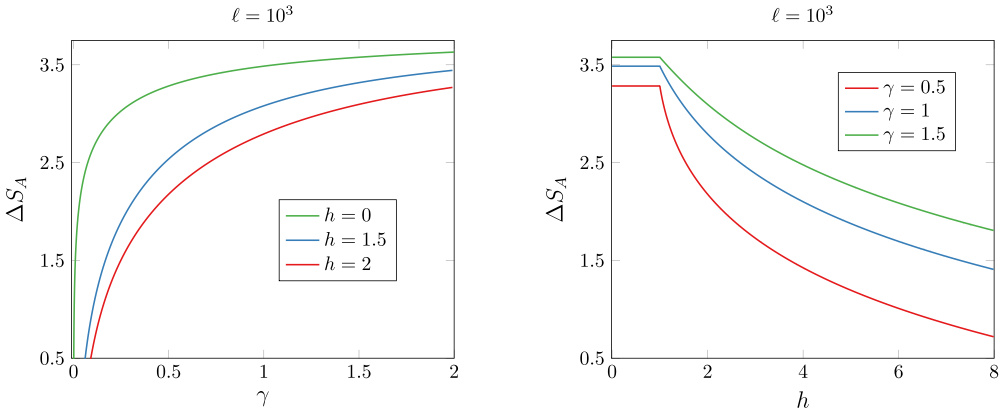

Figure 5. Plot of the asymptotic expression (35) in the limit $n \to 1$ of the entanglement asymmetry for the ground state of the XY spin chain as a function of the anisotropy parameter γ and several values of the external magnetic field h (left panel) and viceversa (right panel). In both plots we take as subsystem length $\ell = 10^3$.

In order to evaluate the time evolution of the entanglement asymmetry in this quench protocol, we first derive a quasi-particle description for the dynamics of the charged moments defined in equation (8).

4.1. Time evolution of the charged moments

In section 3, we have exploited the fact that the reduced density matrix ρ_A of the ground state of the XY spin chain is Gaussian and, in virtue of Wick theorem, the charged moments $Z_n(\boldsymbol{\alpha}, t = 0)$ are univocally determined by the two-point correlation matrix Γ of equation (17). Since the XX Hamiltonian is quadratic in terms of the fermionic operators $\boldsymbol{c}_j$, equation (17) also applies for the reduced density matrix $\rho_A(t)$ of subsystem A after the quench. Furthermore, given that the post-quench Hamiltonian preserves the translational invariance of the system, the time-evolved two-point correlation matrix $\Gamma(t)$ is still block Toeplitz and reads [61]

$$\Gamma_{jj'}(t) = \int_{-\pi}^{\pi} \frac{\mathrm{d}k}{2\pi} \mathrm{e}^{-ik(j-j')} \mathcal{G}(k,t), \quad j, j' = 1, \dots, \ell, \tag{38}$$

where the symbol $\mathcal{G}(k,t)$ is now

$$\mathcal{G}(k,t) = \begin{pmatrix} \cos\Delta_k & -i\,\mathrm{e}^{-2it\epsilon_{\mathrm{XX}}(k)} \sin\Delta_k \\ i\mathrm{e}^{2it\epsilon_{\mathrm{XX}}(k)} \sin\Delta_k & -\cos\Delta_k \end{pmatrix}, \tag{39}$$

with $\cos\Delta_k$ and $\sin\Delta_k$ defined in equation (11) and $\epsilon_{\mathrm{XX}}(k) = -\cos(k)$ is the one-particle dispersion relation of the post-quench Hamiltonian H_{XX}.

In order to find the analytic expression that describes the charged moments $Z_n(\boldsymbol{\alpha}, t)$ in the ballistic regime $t, \ell \to \infty$ with $\zeta = t/\ell$ fixed, we first determine their stationary value at large times. It can be obtained by averaging the time dependent terms in the

symbol $\mathcal{G}(k,t)$ of equation (39). As $t\to\infty$, the terms $\mathrm{e}^{\pm 2it\epsilon_{\rm XX}(k)}$ average to zero and the symbol reduces to

$$\mathcal{G}\left(k,t\to\infty\right)=\begin{pmatrix}\cos\Delta_k & 0\\ 0 & -\cos\Delta_k\end{pmatrix}. \tag{40}$$

Observe that the correlators $\langle\Psi(t)|c_jc_{j'}|\Psi(t)\rangle$ and $\langle\Psi(t)|c_j^\dagger c_{j'}^\dagger|\Psi(t)\rangle$ vanish in the stationary regime. This is the first signature of the dynamical restoration of the particle number symmetry in the subsystem A.

For $n=2$, the stationary behavior of $Z_2(\alpha,t)$ can be determined by applying the conjecture of equation (21), as we did in equation (23) for the charged moments of the ground state. In this case,

$$\log Z_2\left(\alpha,t\to\infty\right)\sim\frac{\ell}{2}\int_0^{2\pi}\frac{\mathrm{d}k}{2\pi}\log\det\left[\frac{I+\mathcal{G}_\alpha\left(k,t\to\infty\right)\mathcal{G}_{-\alpha}\left(k,t\to\infty\right)}{2}\right], \tag{41}$$

and, using the time-averaged symbol of equation (40), we find

$$\log Z_2\left(\alpha,t\to\infty\right)\sim\ell\int_0^{2\pi}\frac{\mathrm{d}k}{2\pi}h_2\left(n\left(k\right)\right), \tag{42}$$

where we have introduced

$$h_n\left(x\right)=\log\left[x^n+\left(1-x\right)^n\right] \tag{43}$$

and $n(k)\equiv\langle\Psi(0)|\mathrm{d}_k^\dagger\mathrm{d}_k|\Psi(0)\rangle=(1-\cos\Delta_k)/2$ is the density of occupied modes with momentum k. This result implies that $Z_2(\alpha,t\to\infty)\sim Z_2(0,t\to\infty)$; in fact, we recover the result predicted in [61] for the stationary value of the entanglement entropy in this quench protocol.

For $n>2$, we cannot employ the conjecture of equation (21) to derive the stationary value of $Z_n(\boldsymbol{\alpha},t)$ at large times. In general, the expression (17) for the charged moments does not simplify as for the case $n=2$, cf equation (18), and it contains the inverse matrix $(I-\Gamma(t))^{-1}$. Nevertheless, in equation (66) of appendix A, we report a formula that predicts the asymptotic behavior of a determinant like the one in equation (17), with a product of block Toeplitz matrices that also includes the inverse of block Toeplitz matrices. Since the time-averaged symbol $I-\mathcal{G}(k,t\to\infty)$ of the matrix $I-\Gamma(t)$ is invertible, we can directly apply equation (66) to (17) in the large time limit,

$$\log Z_n\left(\boldsymbol{\alpha},t\to\infty\right)\sim\frac{\ell}{2}\int_0^{2\pi}\frac{\mathrm{d}k}{2\pi}\log\det\left[\left(\frac{I-\mathcal{G}\left(k,t\to\infty\right)}{2}\right)^n\left(I+\prod_{j=1}^n\mathcal{W}_j\left(k\right)\right)\right], \tag{44}$$

where $\mathcal{W}_j(k)=(I+\mathcal{G}(k,t\to\infty))(I-\mathcal{G}(k,t\to\infty))^{-1}\mathrm{e}^{i\alpha_{j,j+1}\sigma_z}$. Using equation (40) and calculating directly the determinant, we find

J. Stat. Mech. (2024) 013103

$$\log Z_n(\boldsymbol{\alpha}, t\to\infty) \sim \ell \int_0^{2\pi} \frac{\mathrm{d}k}{2\pi} h_n(n(k)), \tag{45}$$

that is, $Z_n(\boldsymbol{\alpha}, t\to\infty) \sim Z_n(\mathbf{0}, t\to\infty)$.

At this point, we know both the charged moments $Z_n(\boldsymbol{\alpha}, t)$ at the initial time from equation (27) and its asymptotic behavior at $t\to\infty$ in equation (45). These two ingredients are enough to reconstruct the dynamics of $Z_n(\boldsymbol{\alpha}, t)$ for any finite time t by exploiting the quasi-particle picture of entanglement. The underlying idea is that the pre-quench initial state has very high energy with respect to the ground state of the Hamiltonian governing the post-quench dynamics; hence, it can be seen as a source of quasi-particle excitations at $t=0$. We assume that quasi-particles are uniformly created in pairs with momenta $\pm k$ and velocity $v(k) = \mathrm{d}\epsilon_{\mathrm{XX}}(k)/\mathrm{d}k$. At a generic time t, the entanglement between a subsystem A and B is proportional to the total number of quasi-particles that were created at the same spatial point and are shared between A and B at that moment, which is given by the function $\min(2t|v(k)|, \ell)$. This idea has been firstly proposed to compute the entanglement dynamics after a global quantum quench in [64–66]. However, we can also apply it here to determine the time evolution of the charged moments $Z_n(\boldsymbol{\alpha}, t)$, in the same way as it was done in [21, 22] for the tilted ferromagnetic and Néel states respectively. If we subtract from the stationary value (45) of $Z_n(\boldsymbol{\alpha}, t)$ its initial asymptotic behavior, obtained in equation (27), we get the contribution to $Z_n(\boldsymbol{\alpha}, t)$ at $t\to\infty$ of the pairs of entangled quasi-particle generated in the quench and shared between A and B,

$$\log\left(\frac{Z_n(\boldsymbol{\alpha}, t\to\infty)}{Z_n(\boldsymbol{\alpha}, t=0)}\right) \sim \log Z_n(\mathbf{0}, t\to\infty) - \ell \int_0^{2\pi} \frac{\mathrm{d}k}{2\pi} \log \prod_{j=1}^{n} f_k(\alpha_{j,j+1}). \tag{46}$$

This expression can be extended to finite times by properly counting the number of entangled excitations that A and B share at each moment. This can be done by simply inserting the function $\min(2\zeta|v(k)|, 1)$ in the momentum integrals of the right hand side of equation (46). We then obtain the exact time evolution after the quench of the charged moments (8) in the scaling limit $t, \ell\to\infty$ with $\zeta = t/\ell$ fixed,

$$Z_n(\boldsymbol{\alpha}, t) = Z_n(\mathbf{0}, t)\, \mathrm{e}^{\ell(A_n(\boldsymbol{\alpha}) + B_n(\boldsymbol{\alpha}, \zeta))}, \tag{47}$$

where $Z_n(\mathbf{0}, t)$ and $B_n(\boldsymbol{\alpha}, \zeta)$ read respectively

$$\log Z_n(\mathbf{0}, t) = \ell \int_0^{2\pi} \frac{\mathrm{d}k}{2\pi} \min(2\zeta|v(k)|, 1)\, h_n(n(k)) \tag{48}$$

and

$$B_n(\boldsymbol{\alpha}, \zeta) = -\int_0^{2\pi} \frac{\mathrm{d}k}{4\pi} \min(2\zeta|v(k)|, 1) \log \prod_{j=1}^{n} f_k(\alpha_{j,j+1}). \tag{49}$$

The coefficient $A_n(\boldsymbol{\alpha})$ is given in equation (28). The expression (47) is the main result of this section, and we benchmark it against exact numerical calculations in figure 6

J. Stat. Mech. (2024) 013103

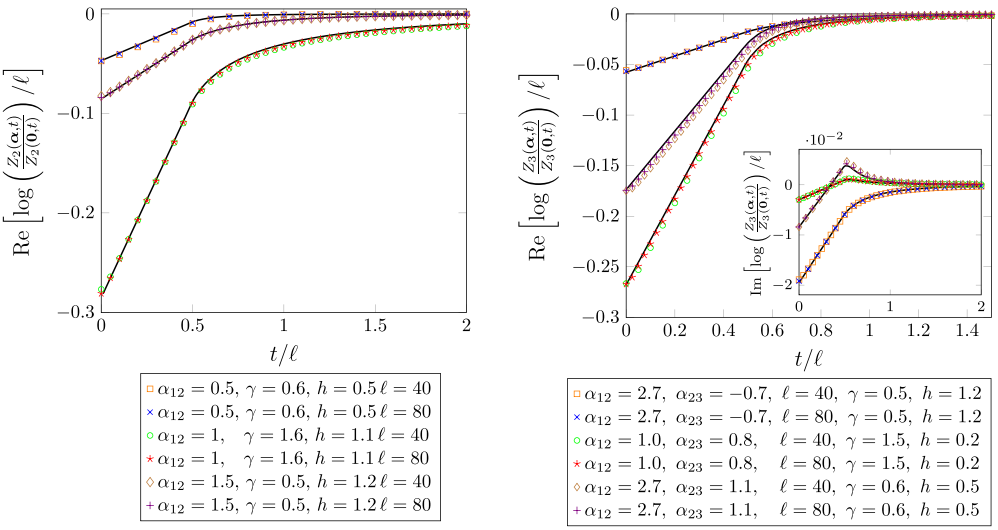

Figure 6. Time evolution of $Z_n(\boldsymbol{\alpha},0)$ after the quench (37) for $n=2$ (left panel) and $n=3$ (right panel). We plot it as a function of t/ℓ taking several initial ground states with different couplings γ,h and various values of the subsystem size ℓ and the phases $\alpha_{j,j+1}$. The symbols were obtained numerically using equation (17) and the continuous lines correspond to the analytic prediction of equation (47).

taking as initial configuration the ground state of the XY spin chain for different values of the couplings γ and h: the symbols have been obtained using equation (17), while the solid lines are equation (47). This expression is valid in the limit $\ell\to\infty$, and we observe that the agreement improves as ℓ increases.

4.2. Time evolution of the entanglement asymmetry

We can now explicitly compute the time evolution of the entanglement asymmetry using the analytic result of the previous section. By plugging equation (47) into equation (7), we obtain $\Delta S_A^{(n)}(t)$ in the scaling limit $t,\ell\to\infty$ with ζ fixed. We show the result in figure 7 for $n=2$ (left top panel) and $n=3$ (left bottom panel) and different choices of the parameters γ and h for the initial state. The agreement between our analytical prediction (solid lines) and the exact numerical computations (symbols) is overall very good in both cases, especially in the top panel, because the system size ℓ is bigger and also larger values of n involve the computation of $n-1$-fold integral (according to equation (7)), so bigger accuracy and precision. Beyond the good matching, we remark that $\Delta S_A^{(n)}(t)$ tends to zero for large time (i.e. large ζ). This is consistent with the fact that when we take the limit $t\to\infty$ in equation (47), the coefficient $B_n(\boldsymbol{\alpha})\to -A_n(\boldsymbol{\alpha})$ and, as we already saw, $Z_n(\boldsymbol{\alpha},t\to\infty)\to Z_n(\mathbf{0},t\to\infty)$. This implies that $\Delta S_A^{(n)}(t\to\infty)\to 0$ and the $U(1)$ symmetry is restored in subsystem A in the stationary regime. This restoration was already observed in [21], see also [67, 68], for the quench from the tilted ferromagnetic state, which is the ground state of the XY spin chain along the curve $\gamma^2+h^2=1$. Another intriguing effect that we observe in figure 7 is that for some pairs of initial parameters, e.g. $\gamma=0.6$, $h=0.5$ and $\gamma=0.5$, $h=0.2$, the curves that the

J. Stat. Mech. (2024) 013103

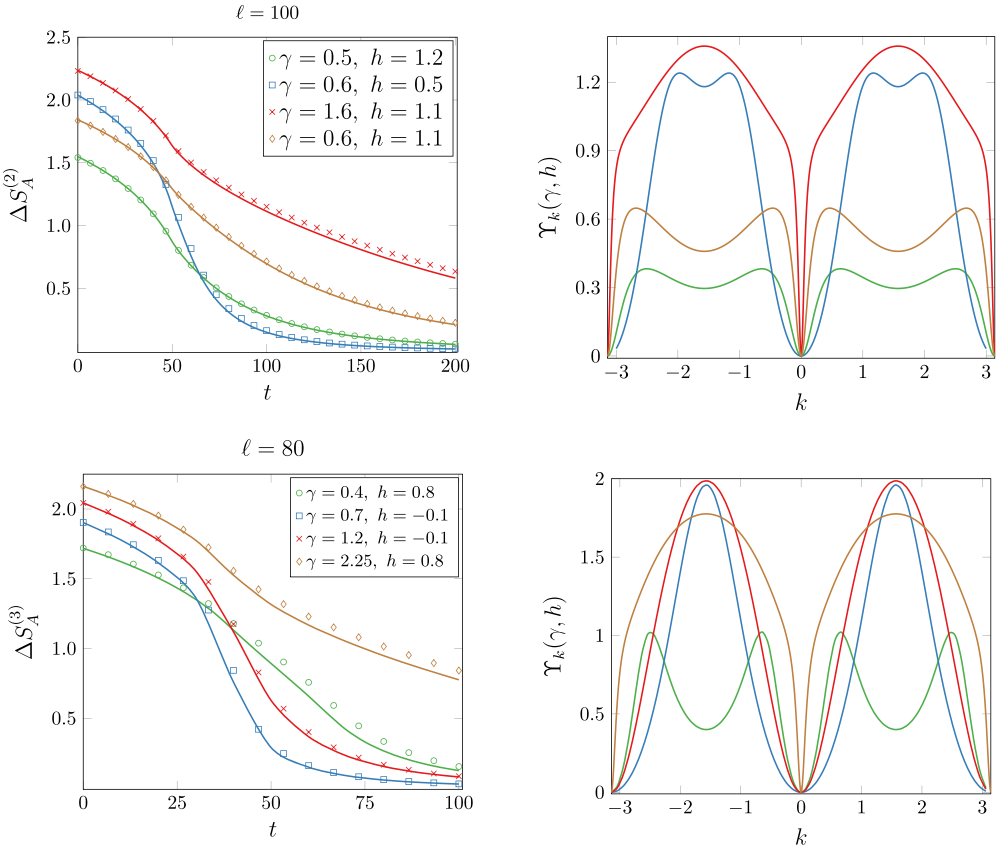

Figure 7. Left panels: time evolution of the Rényi entanglement asymmetry $\Delta S_A^{(n)}(t)$ after the quench (37). The symbols are the exact numerical results for a subsystem of length $\ell = 100$ ($n = 2$) and $\ell = 80$ ($n = 3$), and different initial conditions for γ, h. The continuous lines are our prediction obtained by plugging the charged moments reported in equation (47) into equations (2) and (7). Right panels: square of the density of the Cooper pairs at time $t = 0$ in equation (11). The crossing of two densities is a necessary condition for the presence of quantum Mpemba effect, according to the criterion explained in the main text.

corresponding asymmetry $\Delta S_A^{(n)}(t)$ describes in time cross such that, for the state that initially breaks more the symmetry, the quench restores it earlier. This phenomenon was dubbed quantum Mpemba effect in [21], which states that the more the system is initally out of equilibrium, the faster it relaxes. However, in the left panels of figure 7, we can also see that this effect does not always occur. We can find pairs of initial couplings, e.g. $\gamma = 0.6, h = 0.5$ and $\gamma = 1.6, h = 1.2$, for which there is not a crossing between the curves and the symmetry is restored faster when the symmetry is less broken, i.e. for the smaller value of γ, $\gamma = 0.6$. Let us investigate this phenomenon better to derive a condition under which we expect to observe the quantum Mpemba effect in the quenches (37).

Starting from equation (47), we aim to derive an effective closed-form approximation of $\Delta S_A^{(n)}(t)$ when the exponent in the charged moments $Z_n(\boldsymbol{\alpha}, t)$, $A_n(\boldsymbol{\alpha}) + B_n(\boldsymbol{\alpha}, \zeta)$ is

J. Stat. Mech. (2024) 013103

small, i.e. for large values of time t. By using the Taylor expansion of an exponential function $\mathrm{e}^{f(x)}$ when $f(x) \to 0$, the Fourier transform in equation (7) can be performed analytically in that limit and we find

$$\begin{aligned} \Delta S_A^{(n)}(t) &\simeq \frac{n\ell}{1-n} b(\zeta,\gamma,h), \\ b(\zeta,\gamma,h) &= \int_{-\pi}^{\pi} \frac{\mathrm{d}k}{4\pi} [1 - \min(2\zeta|v(k)|,1)] \log \frac{1+\sqrt{1-\sin^2\Delta_k}}{2}. \end{aligned} \tag{50}$$

This result represents the quasi-particle picture for the entanglement asymmetry in terms of Cooper pairs. As we discussed in section 3, the term $\sin^2\Delta_k$ is identified with the density of Cooper pairs in the initial state, i.e. $\sin^2\Delta_k = |\langle\Psi(0)|\mathrm{d}^\dagger_{\pi-k}\mathrm{d}^\dagger_k|\Psi(0)\rangle|^2$. Therefore, according to equation (50), the entanglement asymmetry vanishes at large times as the number of Cooper pairs in the subsystem A reduces ballistically to zero. This means that the rate at which the symmetry is restored is governed by the modes with the lowest group velocity $v(k)$. This observation is crucial to understand the occurrence of the quantum Mpemba effect.

If we consider two different sets of couplings h_1, γ_1 and h_2, γ_2 for the initial ground state such that

$$\Delta S_A^{(n)}(t=0,\gamma_1,h_1) < \Delta S_A^{(n)}(t=0,\gamma_2,h_2). \tag{51}$$

Then the quantum Mpemba effect occurs when there is a time, that we denote as t_I, after which the initial relation is inverted, i.e.

$$\Delta S_A^{(n)}(t,\gamma_1,h_1) > \Delta S_A^{(n)}(t,\gamma_2,h_2) \qquad \forall t > t_I. \tag{52}$$

We can observe the quantum Mpemba effect if an only if conditions (51) and (52) are satisfied.

Using the asymptotic expression (35) for the ground state of the XY Hamiltonian, the condition (51) at $t=0$ can be rewritten in terms of the density of Cooper pairs of the two initial configurations as

$$\int_{-\pi}^{\pi} \mathrm{d}k \sin^2\Delta_k(\gamma_1,h_1) < \int_{-\pi}^{\pi} \mathrm{d}k \sin^2\Delta_k(\gamma_2,h_2). \tag{53}$$

On the other hand, according to equation (50), the inequality (52) is satisfied if and only if $b(\zeta,\gamma_1,h_1) > b(\zeta,\gamma_2,h_2)$, for all $\zeta > \zeta_I = t_I/\ell$. It is clear that it is sufficient to enforce this second condition only for large times. Let us then study more carefully the behavior of the function $b(\zeta,\gamma_1,h_1)$ in the limit $t \to \infty$ or, equivalently, the limit $\zeta \to \infty$. In this case, it is useful to apply the identity,

$$1 - \min(2\zeta|v(k)|,1) = (1-2\zeta|v(k)|)\,\Theta(1-2\zeta|v(k)|), \tag{54}$$

J. Stat. Mech. (2024) 013103

where Θ is the Heaviside Theta function, such that $\Theta(x)=1$ when $x>0$. Plugging this result in equation (50), we firstly observe that

$$b(\zeta,\gamma,h)=\int_{-\pi}^{\pi}\frac{\mathrm{d}k}{4\pi}\,(1-2\zeta|v(k)|)\,\Theta(1-2\zeta|v(k)|)\log\frac{1+\sqrt{1-\sin^2\Delta_k}}{2}, \quad (55)$$

is non-vanishing for the modes $-\zeta^{-1}<2v(k)<\zeta^{-1}$. At large times, since $|v(k)|=|\sin(k)|$, this condition is satisfied if $k^*(\zeta)=\arcsin(1/(2\zeta))$ exists such that

$$\begin{aligned}b(\zeta,\gamma,h)=&\int_{-k^*(\zeta)}^{k^*(\zeta)}\frac{\mathrm{d}k}{4\pi}\,(1-2\zeta|v(k)|)\log\frac{1+\sqrt{1-\sin^2\Delta_k}}{2}\\&+\int_{\pi-k^*(\zeta)}^{\pi+k^*(\zeta)}\frac{\mathrm{d}k}{4\pi}\,(1-2\zeta|v(k)|)\log\frac{1+\sqrt{1-\sin^2\Delta_k}}{2}.\end{aligned} \quad (56)$$

Outside the critical lines $|h|\neq 1$, $\sin^2\Delta_k$ vanishes around $k=0$ and π and, therefore, we can take the approximation $\log[(1+\sqrt{1-x})/2]\sim -x/4$,

$$b(\zeta,\gamma,h)\simeq-\int_{-k^*(\zeta)}^{k^*(\zeta)}\frac{\mathrm{d}k}{16\pi}\,(1-2\zeta|v(k)|)\sin^2\Delta_k-\int_{\pi-k^*(\zeta)}^{\pi+k^*(\zeta)}\frac{\mathrm{d}k}{16\pi}\,(1-2\zeta|v(k)|)\sin^2\Delta_k. \quad (57)$$

If we perform the change of variables $k'=k-\pi$ in the second integral of the expression above, we then find

$$b(\zeta,\gamma,h)\simeq-\int_{-k^*(\zeta)}^{k^*(\zeta)}\frac{\mathrm{d}k}{16\pi}(1-2\zeta|v(k)|)\Upsilon_k(\gamma,h), \quad (58)$$

where $\Upsilon_k(\gamma,h)=\sin^2\Delta_k(\gamma,h)+\sin^2\Delta_k(\gamma,-h)$.

Therefore, the condition (52), i.e. $b(\zeta,h_1,\gamma_1)>b(\zeta,h_2,\gamma_2)$ for large ζ, to observe the quantum Mpemba effect can be re-expressed in terms of the densities of Cooper pairs in the initial states as

$$\int_{-k^*(\zeta)}^{k^*(\zeta)}\mathrm{d}k\,\Upsilon_k(\gamma_1,h_1)>\int_{-k^*(\zeta)}^{k^*(\zeta)}\mathrm{d}k\,\Upsilon_k(\gamma_2,h_2)\qquad\text{for }\zeta>\zeta_I. \quad (59)$$

Given the form of $\sin^2\Delta_k$, $\Upsilon_k(\gamma,h)$ is a definite positive, even function of k that vanishes at $k=0$ for any value of $\gamma>0$ and $|h|\neq 1$. Therefore, there always exists a large enough time t_I for which the integral condition of equation (59) can be replaced by

$$\Upsilon_k(\gamma_1,h_1)>\Upsilon_k(\gamma_2,h_2),\quad k\in\left[-\arcsin\left(\frac{\ell}{2t_I}\right),\arcsin\left(\frac{\ell}{2t_I}\right)\right]. \quad (60)$$

Equations (53) and (60) are the necessary and sufficient microscopic conditions to observe the quantum Mpemba effect between a pair of ground states of the XY spin chain after a quench to the XX spin chain. According to them, the quantum Mpemba

J. Stat. Mech. (2024) 013103

effect occurs when the state that initially breaks less the symmetry, and therefore contains a smaller net number of Cooper pairs (condition (53)), has instead a larger density of Cooper pairs around the modes with the slowest velocity $v(k)$ (condition (60)), which correspond to the momenta $k=0$ and $k=\pi$. This is a very natural condition since the entanglement asymmetry satisfies the quasi-particle picture of equation (50) and, therefore, its leading behavior at large times is determined by the slowest excitations. In the right panels of figure 7, we plot the function $\Upsilon_k(\gamma,h)$ that enters in the condition (60) for some of the initial states studied in the left panels of that figure: observe that, whenever the inequality (60) is met for a pair of couplings (γ,h) that also satisfy (53), the curves that describe their asymmetries intersect at certain time and equation (52) is fulfilled. Notice that the simultaneous validity of equations (51) and (52) then requires that the density of Cooper pairs corresponding to two different quenches should cross, as made explicit in figure 7. In addition, we observe that the conditions (53) and (59) are valid for any value of the Rényi index n. For the condition at $t=0$, the reason is that all the dependence on γ and h in equation (35) is in the term $g(\gamma,h)$, which is independent of n. For the large time condition, the starting point (50) from which it is derived does not depend on n.

Many of the former considerations are valid generically in integrable systems [23]. Specializing on our quench, we can obtain a set of conditions for the quantum Mpemba effect equivalent to the microscopic ones but only involving the couplings γ, h of the initial states. For the inequality (51) at $t=0$, this can be straightforwardly done using the asymptotic expression (35), together with equation (36) for the term $g(\gamma,h)$. In the case of the condition (52) at large times, we need to determine explicitly the leading behavior of $\Delta S_A^{(n)}(t)$ when $t\to\infty$. For $|h|\neq 1$, this can be done from equation (57) by expanding the functions $v(k)$ and $\sin^2\Delta_k$ around $k=0$ or $k=\pi$ in each integral and $k^*(\zeta)$ around $\zeta=\infty$. We find that, at leading order in large ζ,

$$\Delta S_A^{(n)}(t)=\frac{n}{384\pi\,(n-1)}\frac{\gamma^2\left(h^2+1\right)}{\left(h^2-1\right)^2}\frac{\ell}{\zeta^3}\,, \tag{61}$$

i.e. it vanishes for large times as t^{-3} for any value of γ and h. The fact that the prefactor in equation (61) monotonically increases as a function of γ and it depends non-trivially on h reflects that it is not enough starting from a state with larger γ to reach before $\Delta S_A^{(n)}(t)\to 0$, but the dependence on h is crucial to observe the Mpemba effect. Fixing γ, we notice that, for $|h|<1$, equation (61) is a monotonically increasing function of h; since the initial asymmetry grows with γ and does not depend on h in this region, then it is necessary that $\gamma_2>\gamma_1$ and $h_2<h_1$ to satisfy the Mpemba conditions (51) and (52). In particular, they are always met by any pair of ground states with couplings belonging to the curve $h^2+x\gamma^2=1$ for a fixed parameter $x>0$, which describes an ellipse in the (h,γ)-plane. In fact, for any initial state on this curve,

$$\Delta S_A^{(n)}(t)=\frac{n}{384\pi\,(n-1)\,x}\left(\frac{2}{x\gamma^2}-1\right)\frac{\ell}{\zeta^3}\,. \tag{62}$$

J. Stat. Mech. (2024) 013103

In this case, the prefactor of the t^{-3} decay is a monotonously decreasing function of γ, and, therefore, we always observe that the more the symmetry is broken, the faster it is restored. Interestingly, for large subsystems, the spectrum of the correlation matrix Γ is the same for all the ground states along a curve $h^2 + x\gamma^2 = 1$ and, consequently, they have equal entanglement entropy [69–71]. On the other hand, the discussion in the region $|h| > 1$ is more involved because both the initial entanglement asymmetry (35) and its large time behavior (61) are monotonic decreasing functions of h.

The replica limit $n \to 1$ in equation (61) is not well defined. In appendix B, we carefully perform it, starting from the Fourier transform of the charged moments in equation (7). The final result reads

$$\Delta S_A(t) = -\frac{\gamma^2\left(h^2+1\right)\ell}{384\pi\left(h^2-1\right)^2\zeta^3}\log\left[\frac{\gamma^2\left(h^2+1\right)\ell}{384\pi\left(h^2-1\right)^2\zeta^3}\right]. \tag{63}$$

Observe that, while the Rényi entanglement asymmetry in equation (61) decays to zero at large times as ℓ^4/t^3, in the limit $n \to 1$ it behaves as $\ell^4 \log(t)/t^3$, being the logarithmic correction $\log(t)$ a particular feature of this case. This also happens for the von Neumann entanglement entropy, as it has been found in [61].

When $|h| = 1$, we can find an expression similar to equation (61). In this case, $\sin^2 \Delta_k \neq 0$ at $k = 0$ and the approximation of equation (57) is not valid. If we take equation (56) instead and we expand at leading order the integrands around the modes $k = 0$ and $k = \pi$ respectively and the function $k^*(\zeta)$ around $\zeta = \infty$, then we obtain

$$\Delta S_A^{(n)}(t) = \frac{n}{n-1}\frac{\log 2}{8\pi}\frac{\ell}{\zeta}. \tag{64}$$

We observe that the behavior of the entanglement asymmetry as a function of ζ is different if the initial configuration is the ground state of a critical Hamiltonian or not: in the former case, it decreases as $1/\zeta$, while if we start outside the critical line the decay to zero is algebraically faster, as $1/\zeta^3$. Therefore, if we consider a critical state and a non-critical one that breaks more the symmetry, the symmetry is always restored faster in the latter. This can be seen as a *strong* quantum Mpemba effect. In fact, in the classical Mpemba effect, the system relaxes exponentially to the equilibrium state, but in certain particular situations, the decay is exponentially faster, a phenomenon dubbed as strong Mpemba effect [9]. By analogy, in our quantum setup, the asymmetry reaches the equilibrium always following a power law but with a smaller exponent in the case of critical states, so in a much slower fashion. In addition, note that the prefactor of equation (64) does not depend on γ, while the initial entanglement asymmetry along the lines $|h| = 1$ grows monotonically with γ according to equation (35). This means that, independently of how much the symmetry is initially broken, for critical states, it is restored (almost) at the same time, as we show in figure 8. We can call this phenomenon *weak* quantum Mpemba effect.

J. Stat. Mech. (2024) 013103

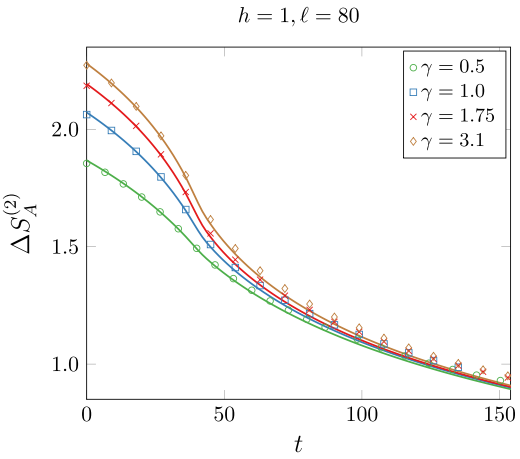

Figure 8. Time evolution of the Rényi entanglement asymmetry $\Delta S_A^{(2)}(t)$ after the quench (37) from a critical state, $h = 1$ and different γ's. The symbols are the exact numerical results for a subsystem of length $\ell = 80$. The continuous lines are our prediction obtained by plugging the charged moments reported in equation (47) into equations (2) and (7). As explained in the main text, whatever is the initial value of γ, for large time t the lines collapse and, eventually, the symmetry is restored almost simultaneously, a weak version of Mpemba effect.

As occurs in the non-critical region, the limit $n \to 1$ in equation (64) is also not well defined. Repeating the same steps as in appendix B for the gapped phase, we find

$$\Delta S_A(t) = -\frac{\ell \log 2}{8\pi\zeta} \log\left[\frac{\ell}{8\pi\zeta}\right], \tag{65}$$

which differs from the result of equation (64) for the Rényi entanglement asymmetry in the logarithmic correction $\log(t)$.

5. Conclusions

In this manuscript, we have investigated the $U(1)$ symmetry breaking in the XY spin chain using the entanglement asymmetry, completing the analysis initiated in [21] for the tilted ferromagnetic state and specializing the general discussion on the quantum Mpemba effect for integrable systems done in [23]. We have first studied the behavior of the entanglement asymmetry in the ground state of this model, finding that, at leading order, it grows logarithmically with the subsystem size whether ($|h| \neq 1$) or not the system is gapped. We remark that this is quite different with respect to what happens for the total entanglement entropy, quantity from which the entanglement asymmetry is defined: when $|h| \neq 1$, the entanglement entropy saturates to a constant value for large subsystems [72, 73], while a violation of the area law occurs only along the critical lines, where the entropy scales logarithmically with the subsystem size [51]. Another important result of this work is that we find that the entanglement asymmetry depends on the density of the Cooper pairs, $|\langle \mathrm{d}_{\pi-k} \mathrm{d}_k \rangle|$, of the ground state. This is a natural

J. Stat. Mech. (2024) 013103

result if we take into account that the breaking of the $U(1)$ particle number symmetry in the XY spin chain can be traced back to the presence of superconducting pairing terms in the corresponding fermionic Hamiltonian.

In addition, we have investigated the evolution of the entanglement asymmetry in a global quantum quench, starting from the ground state of the XY spin chain and letting the system evolve with the XX Hamiltonian that preserves the particle number such that the symmetry is dynamically restored in the subsystem. With the help of the quasi-particle picture of entanglement, we have derived a closed-form analytic expression for the asymmetry at large times, from which we have deduced the necessary and sufficient conditions to observe the quantum Mpemba effect in terms of the density of Cooper pairs of the initial states. Essentially, if the density of the slowest Cooper pairs is larger for the state that breaks less the symmetry, then the Mpemba physics shows up, meaning that the more the symmetry is broken, the faster it is restored. The set of microscopic conditions that we obtain here are in agreement with the criteria derived in [23] for an arbitrary integrable quantum system.

It would be interesting to investigate several questions in the future. The first one is an explanation of the mechanism of the quantum Mpemba effect when the symmetry is restored by a non-integrable Hamiltonian, or the evolution is non-unitary. This analysis has been initiated in [21] for systems of a few sites, showing the robustness of this phenomenon also if the evolution Hamiltonian is non-integrable. So far, only the breaking of Abelian symmetries has been investigated, but we would like to use the entanglement asymmetry to explore the symmetry breaking of non-Abelian groups. Finally, the analysis done in this manuscript has revealed that the critical lines of the XY model, $|h| = 1$, are peculiar since an extra term appears in the charged moments. It would be interesting to find its exact expression and determine its (subleading) contribution to the entanglement asymmetry, not only to have a more accurate prediction of it but also to understand if it contains information about the underlying conformal field theory that describes these critical lines.

Acknowledgments

We thank Bruno Bertini, Katja Klobas and Colin Rylands for useful discussions and collaboration on a related topic [23]. P C and F A acknowledge support from ERC under Consolidator Grant Number 771536 (NEMO). S M thanks support from Caltech Institute for Quantum Information and Matter and the Walter Burke Institute for Theoretical Physics at Caltech. The work of I K was supported in part by the NSF Grant DMR-1918207.

Appendix A. Derivation of the asympotic behavior of the ground state charged moments for integer $n > 2$

In this appendix, we show how to obtain the expression in equation (27) for the charged moments $Z_n(\boldsymbol{\alpha})$ in the ground state of the XY spin chain. Observe that, in general, for $n > 2$ the inverse matrix $(I - \Gamma)^{-1}$ cannot be removed from equation (17) as we did in

equation (18) when $n=2$. In general, the inverse of a block Toeplitz matrix is not block Toeplitz and the result of equation (21) cannot be in principle applied. However, in [22], we found a corollary of equation (21) for the determinant of a product of Toeplitz matrices that involves as well the inverse of block Toeplitz matrices. According to it, if we further include in the determinant of equation (21) the inverse of the block Toeplitz matrices $T_\ell[g_j']$, then for large ℓ,

$$\det\left(I+\prod_{j=1}^{n}T_\ell\left[g_j\right]T_\ell\left[g_j'\right]^{-1}\right)\sim \mathrm{e}^{\ell A'}, \tag{66}$$

where

$$A'=\int_0^{2\pi}\frac{\mathrm{d}k}{2\pi}\log\det\left[I+\prod_{j=1}^{n}g_j\left(k\right)g_j'\left(k\right)^{-1}\right]. \tag{67}$$

However, observe that the symbol of the matrix $I-\Gamma$ is $I-\mathcal{G}$, with $\mathcal{G}$ given by equation (16). This symbol is not invertible and equation (66) cannot be applied. We can bypass this issue by considering the system at finite temperature $1/\beta$ and then take the limit $\beta\to\infty$. In fact, the state of the spin chain at temperature $1/\beta$ is described by the Gibbs ensemble $\rho_\beta=\mathrm{e}^{-\beta H}/Z$, where $Z=\mathrm{Tr}(e^{-\beta H})$. The two-point correlation function Γ_β associated to ρ_β is block Toeplitz with symbol

$$\mathcal{G}_\beta\left(k\right)=\tanh\left(\frac{\beta\epsilon\left(k\right)}{2}\right)\begin{pmatrix}\cos\Delta_k & -i\sin\Delta_k\\ i\sin\Delta_k & -\cos\Delta_k\end{pmatrix}, \tag{68}$$

where $\epsilon(k)$ is the one-particle dispersion relation of the XY spin chain Hamiltonian. Observe that, in the zero temperature limit $\beta\to\infty$, $\mathcal{G}_\beta(k)$ yields the ground state symbol $\mathcal{G}(k)$ reported in equation (16). The advantage of $\mathcal{G}_\beta$ is that $I-\mathcal{G}_\beta$ is invertible and equation (66) can be applied to determine the asymptotic behavior of the charged moments $Z_n(\boldsymbol{\alpha},\beta)$ at finite temperature and large subsystem size ℓ. We find

$$Z_n\left(\boldsymbol{\alpha},\beta\right)=\mathrm{e}^{\ell A_n(\boldsymbol{\alpha},\beta)}, \tag{69}$$

with

$$A_n\left(\boldsymbol{\alpha},\beta\right)=\int_0^{2\pi}\frac{\mathrm{d}k}{4\pi}\log\det\left[\left(\frac{I-\mathcal{G}_\beta\left(k\right)}{2}\right)^n\left(I+\prod_{j=1}^{n}\mathcal{W}_{\beta,j}\left(k\right)\right)\right], \tag{70}$$

where $\mathcal{W}_{\beta,j}(k)$ stands for the 2×2 matrix $\mathcal{W}_{\beta,j}(k)=(I+\mathcal{G}_\beta(k))(I-\mathcal{G}_\beta(k))^{-1}\mathrm{e}^{i\alpha_{jj+1}\sigma_z}$. If we now consider the quotient

$$\frac{Z_n\left(\boldsymbol{\alpha},\beta\right)}{Z_n\left(\mathbf{0},\beta\right)}=\mathrm{e}^{\ell[A_n(\boldsymbol{\alpha},\beta)-A_n(\mathbf{0},\beta)]}, \tag{71}$$

J. Stat. Mech. (2024) 013103

and take the limit $\beta \to \infty$, we find equation (27) with

$$A_n(\boldsymbol{\alpha}) = \lim_{\beta\to\infty} \left[A_n(\boldsymbol{\alpha},\beta) - A_n(\mathbf{0},\beta)\right]. \tag{72}$$

By calculating explicitly the determinant in the integrand of equation (70) for different integer values of n, one can check that this limit actually yields the factorized form of equation (28) for the coefficient $A_n(\boldsymbol{\alpha})$.

Appendix B. Large time behavior of the von Neumann entanglement asymmetry

In equation (61), we notice that the replica limit $n \to 1$ is not well-defined. Therefore, in this appendix, we carefully derive the asymptotic expression in the limit $t \to \infty$ of the entanglement asymmetry (1). As already observed in [23], in this regime we can explicitly compute the Fourier transform in equation (7). Indeed, by expanding the charged moments for small values of $(1 - \min(2\zeta|v(k)|, 1))$ (i.e. large ζ), we find

$$\begin{aligned}\frac{\mathrm{Tr}\left(\rho_{A,Q}^n\right)}{\mathrm{Tr}\left(\rho_A^n\right)} &= \int_{-\pi}^{\pi} \frac{\mathrm{d}\alpha_1 \dots \mathrm{d}\alpha_n}{(2\pi)^n} \exp\left[\ell \int_{-\pi}^{\pi} \frac{\mathrm{d}k}{4\pi} \left(1 - \min\left(2\zeta|v(k)|, 1\right)\right) \log \prod_{j=1}^{n} f_k\left(\alpha_{j,j+1}\right)\right] \\ &\simeq 1 + \ell \int_{-\pi}^{\pi} \frac{\mathrm{d}\alpha_1 \dots \mathrm{d}\alpha_n}{(2\pi)^n} \int_{-\pi}^{\pi} \frac{\mathrm{d}k}{4\pi} \left(1 - \min\left(2\zeta|v(k)|, 1\right)\right) \log \prod_{j=1}^{n} f_k\left(\alpha_{j,j+1}\right).\end{aligned} \tag{73}$$

The integral above has been done in equation [sm-54] of [23], and, by identifying $\max[\vartheta(k), 1-\vartheta(k)] = (1+\sqrt{1-\sin^2\Delta_k})/2$ and $\min[\vartheta(k), 1-\vartheta(k)] = (1-\sqrt{1-\sin^2\Delta_k})/2$, we can report here the final result in our case,

$$\begin{aligned}\frac{\mathrm{Tr}\left(\rho_{A,Q}^n\right)}{\mathrm{Tr}\left(\rho_A^n\right)} \simeq &\left(1 + \ell \int_{-\pi}^{\pi} \frac{\mathrm{d}k}{4\pi} \left(1 - \min\left(2\zeta|v(k)|, 1\right)\right) \log \frac{1+\sqrt{1-\sin^2\Delta_k}}{2}\right)^n \\ &+ \sum_{j=-\infty}^{-1} \left[(-1)^j \frac{\ell}{j} \int_{-\pi}^{\pi} \frac{\mathrm{d}k}{4\pi} \left(1 - \min\left(2\zeta|v(k)|, 1\right)\right) \left(\frac{1+\sqrt{1-\sin^2\Delta_k}}{1-\sqrt{1-\sin^2\Delta_k}}\right)^j\right]^n.\end{aligned} \tag{74}$$

We can deduce the replica limit $n \to 1$ after doing an analytic continuation of the result above to any complex value of n and, in the large time regime, we find

$$\begin{aligned}\Delta S_A(t) &= -\lim_{n\to 1} \partial_n \frac{\mathrm{Tr}\left(\rho_{A,Q}^n\right)}{\mathrm{Tr}\left(\rho_A^n\right)} \\ &\simeq -\sum_{j=-\infty}^{-1} (-1)^j \left[\frac{\ell}{j} \int_{-\pi}^{\pi} \frac{\mathrm{d}k}{4\pi} \left(1 - \min\left(2\zeta|v(k)|, 1\right)\right) \left(\frac{1+\sqrt{1-\sin^2\Delta_k}}{1-\sqrt{1-\sin^2\Delta_k}}\right)^j\right. \\ &\quad \left. \times \log\left((-1)^j \frac{\ell}{j} \int_{-\pi}^{\pi} \frac{\mathrm{d}k}{4\pi} \left(1 - \min\left(2\zeta|v(k)|, 1\right)\right) \left(\frac{1+\sqrt{1-\sin^2\Delta_k}}{1-\sqrt{1-\sin^2\Delta_k}}\right)^j\right)\right].\end{aligned} \tag{75}$$

J. Stat. Mech. (2024) 013103

If t is sufficiently large, then $(1-\min(2\zeta|v(k)|,1))$ becomes zero everywhere, except for a finite interval around the points $k=0,\pi$ where the magnitude of the velocity is minimal. Therefore, since we are interested in the leading order behavior in ζ, we can restrict the sum in equation (75) to $j=-1$. Moreover, by expanding $k^*(\zeta)\sim 1/(2\zeta)$ for large ζ and $\sin^2\Delta_k$ around $k=0,\pi$, we obtain for $|h|\neq 1$

$$\int_{-k^*(\zeta)}^{k^*(\zeta)}\frac{\mathrm{d}k}{16\pi}(1-2|k|\zeta)\Upsilon_{k\simeq 0}(\gamma,h)=\frac{\gamma^2\left(h^2+1\right)}{384\pi\left(h^2-1\right)^2\zeta^3}, \tag{76}$$

and, finally, we get equation (63) of the main text.

Along the critical lines $|h|=1$, close to $k=0$, we find

$$\frac{1+\sqrt{1-\sin^2\Delta_k}}{1-\sqrt{1-\sin^2\Delta_k}}=1+O\left(k\right). \tag{77}$$

Therefore, the main difference with respect to the non-critical case is that the leading term at large ζ in the series of equation (75) is not $j=-1$ but we have now to consider all of them. By taking into account that $\sum_{j=-\infty}^{-1}(-1)^j/j=\log 2$, we obtain at leading order in ζ

$$\Delta S_A\left(t\right)\simeq-\ell\log\left(2\right)\left[\int_{-k^*(\zeta)}^{k^*(\zeta)}\frac{\mathrm{d}k}{4\pi}\left(1-2|k|\zeta\right)\right]\times\log\left[\ell\int_{-k^*(\zeta)}^{k^*(\zeta)}\frac{\mathrm{d}k}{4\pi}\left(1-2|k|\zeta\right)\right], \tag{78}$$

from which equation (65) is derived.

Appendix C. Comparison between the charged moments $Z_n(\alpha)$ and the full counting statistics (FCS)

The expression for the charged moments in equation (8) when $n=1$ is also known as FCS, $\chi(\alpha)=\mathrm{Tr}(\rho_A\mathrm{e}^{i\alpha Q_A})$, see [74–78] for different studies of it in the XY spin chain. Given the result for generic n in equation (27) for the ground state, one might be tempted to deduce that, if the $U(1)$ symmetry is broken, the charged moments $Z_n(\boldsymbol{\alpha})$ factorize into the product of the FCS with different phases $\alpha_{j,j+1}$. However, using the results for the FCS obtained in [74, 78], we will show in the following that this is not always true.

The FCS can be cast as the determinant of a Toeplitz matrix with symbol $f(\mathrm{e}^{i\Delta_k},\alpha/2)$ [74, 78], where the function f is given in equation (26). Thus one can use the theorems on the asymptotic behavior of Toeplitz determinants to analyze $\chi(\alpha)$ for $\ell\gg 1$. For $|h|>1$ and any value of α or when $h<1$ and $\alpha\in(-\pi/2,\pi/2)$, the symbol $f(\mathrm{e}^{i\Delta_k},\alpha/2)$ is a non-zero continuous function in k and the Szegő theorem holds,

$$\log\chi\left(\alpha\right)\sim\ell\int_0^{2\pi}\frac{\mathrm{d}k}{2\pi}\log f\left(\mathrm{e}^{i\Delta_k},\frac{\alpha}{2}\right). \tag{79}$$

J. Stat. Mech. (2024) 013103

We observe that the integral satisfies the following equality

$$\int_0^{2\pi}\frac{\mathrm{d}k}{2\pi}\log f\left(\mathrm{e}^{i\Delta_k},\frac{\alpha}{2}\right)=\int_0^{2\pi}\frac{\mathrm{d}k}{4\pi}\log f\left(\cos\left(i\Delta_k\right),\alpha\right), \tag{80}$$

which implies that, in this regime of the parameters, the result in equation (27) is a factorization of the charged moments into the FCS. However, when $|h|<1$ and $\alpha\in[-\pi,-\pi/2]\cup[\pi/2,\pi]$, the symbol $f(\mathrm{e}^{i\Delta_k},\alpha)$ acquires winding number $+1$. In this case, the prediction in equation (79) is not valid and it must be modified as

$$\log\chi\left(\alpha\right)\sim\ell\left(\int_0^{2\pi}\frac{\mathrm{d}k}{2\pi}\log\left[\mathrm{e}^{-ik}f\left(\mathrm{e}^{i\Delta_k},\frac{\alpha}{2}\right)\right]+\log\left(-z_0\right)\right). \tag{81}$$

If we consider the analytic continuation of $f(\mathrm{e}^{i\Delta_k},\alpha)$ from the unit circle $z=\mathrm{e}^{ik}$ to the complex plane, then z_0 denotes the zero of such analytic continuation with $|z_0|<1$ and closest to the unit circle $z=\mathrm{e}^{ik}$. This point can be either

$$z_0=\frac{h+\sqrt{h^2+\gamma^2-1}}{1+\gamma},\quad\text{or}\quad z_0=\frac{h+\sqrt{h^2+\gamma^2\cos^2\left(\alpha\right)-1}}{1-\gamma\cos\left(\alpha\right)}. \tag{82}$$

The presence of this winding number is the responsible that the charged moments $Z_n(\boldsymbol{\alpha})$ do not *exactly* factorize when $\ell\to\infty$ into the FCS $\mathrm{Tr}(\rho_A\mathrm{e}^{i\alpha_{j,j+1}Q_A})$. In other words, if we compare equation (27) with (79) and (81), the factorization only works in principle when $\alpha_{j,j+1}\in(-\pi/2,\pi/2)$ for all j. But taking into account the periodicity properties in $\alpha_{j,j+1}$ of the charged moments, it can be extended to $\alpha_{j,j+1}\in[-\pi,\pi]$ by introducing the parameter σ_j, which vanishes if $|\alpha_{j,j+1}|\leqslant\pi/2$ and $\sigma_j=\pi$ otherwise, i.e. we can write

$$Z_n\left(\boldsymbol{\alpha}\right)\sim Z_n\left(\mathbf{0}\right)\prod_{j=1}^{n}\mathrm{e}^{i\sigma_j/2}\mathrm{Tr}\left(\rho_A\mathrm{e}^{i(\alpha_{j,j+1}-\sigma_j)Q_A}\right). \tag{83}$$

The term $\sigma_j=\pi$ ensures that we are always in the regime where equation (79) is valid.

The Fourier transform of the FCS yields the probability distribution $p(q)$ for the transverse magnetization Q_A (or particle number) to take the value q. We can make a comparison between our final result in equation (35) and the Rényi-Shannon entropy for the distribution $p(q)$, or Rényi number entropy,

$$H_n=\frac{1}{1-n}\log\sum_q p\left(q\right)^n, \tag{84}$$

where $p(q)$ is the probability for the observable Q_A to take the value q. The result for H_n reads

$$H_n=\frac{1}{2}\log\ell+O\left(1\right), \tag{85}$$

where the $O(1)$ term does depend on (γ,h) and, in general, it is different with respect to what we find in equation (35). In fact, it is clear from that expression that the

J. Stat. Mech. (2024) 013103

entanglement asymmetry only takes into account the number of Cooper pairs as the $O(1)$ term only depends on $\sin\Delta_k$, and not on the total number of fermions which contribute to H_n.

References

[1] Mpemba E B and Osborne D G 1969 Cool? *Phys. Educ.* **4** 172
[2] Ahn Y H, Kang H, Koh D Y and Lee H 2016 Experimental verifications of Mpemba-like behaviors of clathrate hydrates *Korean J. Chem. Eng.* **33** 1903
[3] Hu C, Li J, Huang S, Li H, Luo C, Chen J, Jiang S and An L 2018 Conformation directed Mpemba effect on polylactide crystallization *Cryst. Growth Des.* **18** 5757
[4] Chaddah P, Dash S, Kumar K and Banerjee A 2010 Overtaking while approaching equilibrium (arXiv:1011.3598)
[5] Greaney P A, Lani G, Cicero G and Grossman J C 2011 Mpemba-like behavior in carbon nanotube resonators *Metall. Mater. Trans.* A **42** 3907
[6] Lasanta A, Vega Reyes F, Prados A and Santos A 2017 When the Hotter cools more quickly: Mpemba effect in granular fluids *Phys. Rev. Lett.* **119** 148001
[7] Keller T, Torggler V, Jäger S B, Schütz S, Ritsch H and Morigi G 2018 Quenches across the self-organization transition in multimode cavities *New J. Phys.* **20** 025004
[8] Lu Z and Raz O 2017 Nonequilibrium thermodynamics of the Markovian Mpemba effect and its inverse *Proc. Natl Acad. Sci.* **114** 5083
[9] Klich I, Raz O, Hirschberg O and Vucelja M 2019 The Mpemba index and anomalous relaxation *Phys. Rev.* X **9** 021060
[10] Kumar A and Bechhoefer J 2020 Exponentially faster cooling in a colloidal system *Nature* **584** 64
[11] Walker M R and Vucelja M 2022 Mpemba effect in terms of mean first passage time (arXiv:2212.07496)
[12] Teza G, Yaacobu R and Raz O 2023 Relaxation shortcuts through boundary coupling *Phys. Rev. Lett.* **131** 017101
[13] Walker M R, Bera S and Vucelja M 2023 Optimal transport and anomalous thermal relaxations (arXiv:2307.16103)
[14] Bera S, Walker M R and Vucelja M 2023 Effect of dynamics on anomalous thermal relaxations and information exchange (arXiv:2308.04557)
[15] Nava A and Fabrizio M 2019 Lindblad dissipative dynamics in the presence of phase coexistence *Phys. Rev.* B **100** 125102
[16] Kochsiek S, Carollo F and Lesanovsky I 2022 Accelerating the approach of dissipative quantum spin systems towards stationarity through global spin rotations *Phys. Rev.* A **106** 012207
[17] Carollo F, Lasanta A and Lesanovsky I 2021 Exponentially accelerated approach to stationarity in Markovian open quantum systems through the Mpemba effect *Phys. Rev. Lett.* **127** 060401
[18] Manikandan S K 2021 Equidistant quenches in few-level quantum systems *Phys. Rev. Res.* **3** 043108
[19] Ivander F, Anto-Sztrikacs N and Segal D 2023 Hyper-acceleration of quantum thermalization dynamics by bypassing long-lived coherences: an analytical treatment *Phys. Rev.* E **108** 014130
[20] Chatterjee A K, Takada S and Hayakawa H 2023 Quantum Mpemba effect in a quantum dot with reservoirs *Phys. Rev. Lett.* **131** 080402
[21] Ares F, Murciano S and Calabrese P 2023 Entanglement asymmetry as a probe of symmetry breaking *Nat. Commun.* **14** 2036
[22] Ares F, Murciano S, Vernier E and Calabrese P 2023 Lack of symmetry restoration after a quantum quench: an entanglement asymmetry study *SciPost Phys.* **15** 089
[23] Rylands C, Klobas K, Ares F, Calabrese P, Murciano S and Bertini B 2023 Microscopic origin of the quantum Mpemba effect in integrable systems (arXiv:2310.04419)
[24] Bertini B, Klobas K, Collura M, Calabrese P and Rylands C 2023 Dynamics of charge fluctuations from asymmetric initial states (arXiv:2306.12404)
[25] Joshi L K *et al* 2024 Observing the quantum Mpemba effect in quantum simulations (arXiv:2401.04270)
[26] Ferro F, Ares F and Calabrese P 2023 Non-equilibrium entanglement asymmetry for discrete groups: the example of the XY spin chain (arXiv:2307.06902)
[27] Capizzi L and Mazzoni M 2023 Entanglement asymmetry in the ordered phase of many-body systems: the Ising Field Theory *J. High Energy Phys.* **2023** 144

J. Stat. Mech. (2024) 013103

[28] Capizzi L and Vitale V 2023 A universal formula for the entanglement asymmetry of matrix product states (arXiv:2310.01962)
[29] Klich I and Levitov L S 2008 Scaling of entanglement entropy and superselection rules (arXiv:0812.0006)
[30] Laflorencie N and Rachel S 2014 Spin-resolved entanglement spectroscopy of critical spin chains and Luttinger liquids *J. Stat. Mech.* P11013
[31] Goldstein M and Sela E 2018 Symmetry-resolved entanglement in many-body systems *Phys. Rev. Lett.* **120** 200602
[32] Xavier J C, Alcaraz F C and Sierra G 2018 Equipartition of the entanglement entropy *Phys. Rev.* B **98** 041106
[33] Cornfeld E, Goldstein M and Sela E 2018 Imbalance entanglement: symmetry decomposition of negativity *Phys. Rev.* A **98** 032302
[34] Murciano S, Bonsignori R and Calabrese P 2021 Symmetry decomposition of negativity of massless free fermions *SciPost Phys.* **10** 111
[35] Capizzi L and Calabrese P 2021 Symmetry resolved relative entropies and distances in conformal field theory *J. High Energy Phys.* JHEP10(2021)195
[36] Di Giulio G and Erdmenger J 2023 Symmetry-resolved modular correlation functions in free fermionic theories *J. High Energy Phys.* JHEP07(2023)058
[37] Bonsignori R, Ruggiero P and Calabrese P 2019 Symmetry resolved entanglement in free fermionic systems *J. Phys. A: Math. Theor.* **52** 475302
[38] Murciano S, Di Giulio G and Calabrese P 2020 Entanglement and symmetry resolution in two dimensional free quantum field theories *J. High Energy Phys.* JHEP08(2020)073
[39] Parez G, Bonsignori R and Calabrese P 2021 Quasiparticle dynamics of symmetry resolved entanglement after a quench: the examples of conformal field theories and free fermions *Phys. Rev.* B **103** L041104
[40] Parez G, Bonsignori R and Calabrese P 2021 Exact quench dynamics of symmetry resolved entanglement in a free fermion chain *J. Stat. Mech.* 093102
[41] Piroli L, Vernier E, Collura M and Calabrese P 2022 Thermodynamic symmetry resolved entanglement entropies in integrable systems *J. Stat. Mech.* 073102
[42] Bertini B, Calabrese P, Collura M, Klobas K and Rylands C 2023 Nonequilibrium full counting statistics and symmetry-resolved entanglement from space-time duality *Phys. Rev. Lett.* **131** 140401
[43] Murciano S, Alba V and Calabrese P 2023 Symmetry-resolved entanglement in fermionic systems with dissipation *J. Stat. Mech* 2023 113102
[44] Lukin A, Rispoli M, Schittko R, Tai M E, Kaufman A M, Choi S, Khemani V, Leonard J and Greiner M 2019 Probing entanglement in a many-body localized system *Science* **364** 6437
[45] Azses D, Haenel R, Naveh Y, Raussendorf R, Sela E and Dalla Torre E G 2020 Identification of symmetry-protected topological states on noisy quantum computers *Phys. Rev. Lett.* **125** 120502
[46] Neven A *et al* 2021 Symmetry-resolved entanglement detection using partial transpose moments *npj Quantum Inf.* **7** 1
[47] Vitale V, Elben A, Kueng R, Neven A, Carrasco J, Kraus B, Zoller P, Calabrese P, Vermersch B and Dalmonte M 2022 Symmetry-resolved dynamical purification in synthetic quantum matter *SciPost Phys.* **12** 106
[48] Rath A, Vitale V, Murciano S, Votto M, Dubail J, Kueng R, Branciard C, Calabrese P and Vermersch B 2023 Entanglement barrier and its symmetry resolution: theory and experiment *PRX Quantum* **4** 010318
[49] Ma Z, Han C, Meir Y and Sela E 2022 Symmetric inseparability and number entanglement in charge conserving mixed states *Phys. Rev.* A **105** 042416
[50] Holzhey C, Larsen F and Wilczek F 1994 Geometric and renormalized entropy in conformal field theory *Nucl. Phys.* B **424** 443
[51] Calabrese P and Cardy J 2004 Entanglement entropy and quantum field theory *J. Stat. Mech.* P06002
[52] Vermersch B, Elben A, Sieberer L M, Yao N Y and Zoller P 2019 Probing scrambling using statistical correlations between randomized measurements *Phys. Rev.* X **9** 021061
[53] Brydges T, Elben A, Jurcevic P, Vermersch B, Maier C, Lanyon B P, Zoller P, Blatt R and Roos C F 2019 Probing entanglement entropy via randomized measurements *Science* **364** 260
[54] Huang H-Y, Kueng R and Preskill J 2020 Predicting many properties of a quantum system from very few measurements *Nat. Phys.* **16** 1050
[55] Elben A, Flammia S T, Huang H-Y, Kueng R, Preskill J, Vermersch B and Zoller P 2023 The randomized measurement toolbox *Nat. Rev. Phys.* **5** 9
[56] Han C, Meir Y and Sela E 2023 Realistic protocol to measure entanglement at finite temperatures *Phys. Rev. Lett.* **130** 136201
[57] Kurmann J, Thomas H and Müller G 1982 Antiferromagnetic long-range order in the anisotropic quantum spin chain *Physica* A **112** 235

J. Stat. Mech. (2024) 013103

[58] Müller G and Shrock R E 1985 Implications of direct-product ground states in the one- dimensional quantum XYZ and XY spin chains *Phys. Rev.* B **32** 5845
[59] Lieb E, Schultz T and Mattis D 1961 Two soluble models of an antiferromagnetic chain *Ann. Phys., NY* **16** 407
[60] Peschel I 2003 Calculation of reduced density matrices from correlation functions *J. Phys. A: Math. Gen.* **36** L205
[61] Fagotti M and Calabrese P 2008 Evolution of entanglement entropy following a quantum quench: analytic results for the XY chain in a transverse magnetic field *Phys. Rev.* A **78** 010306(R)
[62] Fagotti M and Calabrese P 2010 Entanglement entropy of two disjoint blocks in XY chains *J. Stat. Mech.* P04016
[63] Balian R and Brezin E 1969 Nonunitary Bogoliubov transformations and extension of Wick's theorem *Nuovo Cimento* B **64** 37
[64] Calabrese P and Cardy J 2005 Evolution of entanglement entropy in one-dimensional systems *J. Stat. Mech.* P04010
[65] Alba V and Calabrese P 2017 Entanglement and thermodynamics after a quantum quench in integrable systems *Proc. Natl Acad. Sci.* **114** 7947
[66] Alba V and Calabrese P 2018 Entanglement dynamics after quantum quenches in generic integrable systems *SciPost Phys.* **4** 017
[67] Fagotti M, Collura M, Essler F H L and Calabrese P 2014 Relaxation after quantum quenches in the spin-1/2 Heisenberg XXZ chain *Phys. Rev.* B **89** 125101
[68] Piroli L, Vernier E and Calabrese P 2016 Exact steady states for quantum quenches in integrable Heisenberg spin chains *Phys. Rev.* B **94** 054313
[69] Franchini F, Its A R, Jin B-Q and Korepin V E 2007 Ellipses of constant entropy in the XY spin chain *J. Phys. A: Math. Theor.* **40** 8467
[70] Ares F, Esteve J G, Falceto F and De Queiroz A R 2016 On the Möbius transformation in the entanglement entropy of fermionic chains *J. Stat. Mech.* 043106
[71] Ares F, Esteve J G, Falceto F and De Queiroz A R 2017 Entanglement entropy and Möbius transformations for critical fermionic chains *J. Stat. Mech.* 063104
[72] Peschel I 2004 On the entanglement entropy for a XY spin chain *J. Stat. Mech.* P12005
[73] Its A R, Jin B-Q and Korepin V E 2005 Entanglement in XY spin chain *J. Phys. A: Math. Gen.* **38** 2975
[74] Cherng R W and Demler E 2007 Quantum noise analysis of spin systems realized with cold atoms *New J. Phys.* **9** 7
[75] Ivanov D A and Abanov A G 2013 Characterizing correlations with full counting statistics: classical Ising and quantum XY spin chains *Phys. Rev.* E **87** 022114
[76] Stéphan J-M 2014 Emptiness formation probability, Toeplitz determinants and conformal field theory *J. Stat. Mech.* P05010
[77] Groha S, Essler F H L and Calabrese P 2018 Full counting statistics in the transverse field Ising chain *SciPost Phys.* **4** 043
[78] Ares F, Rajabpour M A and Viti J 2021 Exact full counting statistics for the staggered magnetization and the domain walls in the XY spin chain *Phys. Rev.* E **103** 042107

J. Stat. Mech. (2024) 013103